TEX Format Date: July 29, 1996; Time: 8:10

AUTHOR Page Proof

THE SURFACES OF PLUTO AND CHARON

DALE P. CRUIKSHANK, TED L. ROUSH and JEFFREY M. MOORE
NASA Ames Research Center

MARK V. SYKES
University of Arizona

TOBIAS C. OWEN
University of Hawaii

MARY JANE BARTHOLOMEW
NASA Ames Research Center

ROBERT H. BROWN
Jet Propulsion Laboratory

and

KIMBERLY A. TRYKA
Northern Arizona University

Much of the surface of Pluto consists of high-albedo regions covered to an unknown depth by β-N_2 contaminated with CH_4, CO, and other molecules. A portion of the exposed surface appears to consist of solid H_2O. The remainder is covered by lower albedo material of unknown composition. The N_2 ice may occur as polar caps of large extent, leaving ices and other solids of lower volatility in the equatorial regions. The low-albedo material found primarily in the equatorial regions may consist in part of solid hydrocarbons and nitriles produced from N_2 and CH_4 in the atmosphere or in the surface ices. Alternatively, it may arise from deposition from impacting bodies and/or the chemistry of the impact process itself. Charon's surface is probably more compositionally uniform than that of Pluto, and is covered by H_2O ice with possible contaminants or exposures of other materials that are as yet unidentified. The molecular ices discovered on Pluto and Charon have been identified from near-infrared spectra obtained with Earth-based telescopes. The quantitative interpretation of those data has been achieved through the computation of synthetic spectra using the Hapke scattering theory and the optical constants of various ices observed in the laboratory. Despite limitations imposed by the availability of laboratory data on ices in various mixtures, certain specific results have been obtained. It appears that CH_4 and CO are trace constituents, and that some fraction of the CH_4 (and probably the CO) on Pluto is dissolved in the matrix of solid N_2. Pure CH_4 probably also

occurs on Pluto's surface, allowing direct access to the atmosphere. Study of the nitrogen absorption band at 2.148 μm shows that the temperature of the N_2 in the present epoch is 40±2 K. The global temperature regime of Pluto can be modeled from observations of the thermal flux at far-infrared and millimeter wavelengths. The low-albedo equatorial regions must be significantly warmer than the polar regions covered by N_2 (at T = 40 K) to account for the total thermal flux measured. At the present season, the diurnal skin depth of the insolation-driven thermal wave is small, and the observed mm-wave fluxes may arise from a greater depth. Alternatively, the mm-wave flux may arise from the cool, sublimation source region. The surface microstructure in the regions covered by N_2 ice is likely governed by the sintering properties of this highly volatile material. The observed nitrogen infrared band strength requires that expanses of the surface be covered with cm-size crystals of N_2. Grains of H_2O ice on Charon, in contrast, are probably of order 50 μm in size, and do not metamorphose into larger grains at a significant rate. Because of the similarities in size, density, atmosphere, and surface composition between Pluto and Neptune's satellite Triton, the surface structures observed by Voyager on Triton serve as a plausible paradigm for what might be expected on Pluto. Such crater forms, tectonic structures, aeolian features, cryovolcanic structures, and sublimation-degraded topography as are eventually observed on Pluto and Charon by spacecraft will give information on their interior compositions and structures, as well as on the temperature and wind regimes over the planet's extreme seasonal cycle.

I. INTRODUCTION

The surfaces of Pluto and Charon can be described in terms of their chemical/mineralogical compositions, microstructural properties, thermal properties, and their geology, all of which are considered in this chapter. Telescopic observations have given direct information on the compositions and temperatures, while inferences drawn concerning the geology and microstructural properties come primarily from icy bodies elsewhere in the solar system that have been observed at close range by flyby spacecraft, notably Voyager.

Information about Pluto and Charon has come in a discontinuous and somewhat disorderly fashion, as described in the chapter by Marcialis. For instance, in the mid-1970s the existence of Pluto's satellite was unknown. Neither did we know the mass, diameter, or density of Pluto within useful bounds. The planet's photometric lightcurve had been established, indicating a rotation period of 6.390±0.003 days (Hardie 1965). In 1976, the detection of an absorption band in the near-infrared and its identification as due to solid methane (Cruikshank et al. 1976), suggested that Pluto's surface has a high albedo more characteristic of ice than of rock. This inference, in turn, showed that Pluto's diameter is less than that of the Moon, while the dominance of a volatile on the surface suggested that the bulk density might be less than that of pure rock or rock-plus-iron.

Two years later, Christy and Harrington (1978) discovered Charon, the mass of Pluto was determined, and the stage was set for the epoch of mutual transits and eclipses in the mid-1980s which would yield vital information on the dimensions and composition of the Pluto–Charon system (chapter by

Binzel et al.).

Soon after Charon's discovery, near-infrared (0.9–2.5 μm) spectroscopic observations confirmed the identification of frozen methane on Pluto (Cruikshank and Silvaggio 1980; Soifer et al. 1980). Fink et al. (1980) and Apt et al. (1983) observed Pluto's spectrum in the region 0.6 to 1.0 μm, finding additional methane bands, while Buie and Fink (1984) showed that the band strengths vary in phase with the planet's lightcurve, indicating that the methane is not uniformly distributed on the surface. Marcialis and Lebofsky (1991) found the same correlation in spectra in the 0.95 to 2.5 μm region, showing that at lightcurve minimum (maximum exposure of low-albedo surface material) the methane bands are weakest. Unpublished spectra by Cruikshank and Brown also showed the correlation of methane band strength with lightcurve phase. Sawyer (1989) briefly reported that he had seen no significant CH_4 band variation with rotation, and concluded that the absorption was atmospheric, contrary to the results of most of the other investigators. See also the results by Grundy (1995) in Sec. II.B.1. The spectrophotometry by Marcialis and Lebofsky (1991) gives evidence that the darker equatorial region of Pluto is redder in color than the higher albedo regions, a result corroborated by Grundy (1995), and which is consistent with the results of mapping of Pluto's surface reported elsewhere in this book.

In a review of the available near-infrared spectrophotometry of Pluto (+Charon), Clark et al. (1986) suggested that solid or liquid N_2 might be present (because of Pluto's low temperature and because condensed N_2 had been seen in Triton's specrum, though its absorption band could not be discerned in the Pluto data of the time. They also suggested that H_2O ice might be present on the basis of its contribution to the infrared spectral absorption seen on Pluto. Solid N_2 has indeed been found (Owen et al. 1993*a*), and data obtained in 1995 establish the presence of frozen H_2O (Owen et al. 1996). Spencer et al. (1990) used narrowband filters to detect for the first time the strong CH_4 ice band near 3.25 μm.

The break-through discovery relating to the composition of the surface of Charon came during the season of mutual transits and eclipses, when H_2O ice was discovered by spectrophotometry in the near-infrared (Buie et al. 1987; Marcialis et al. 1987). We discuss this more fully below.

Discoveries affecting our understanding of Pluto's surface were the observational detection of the planet's atmosphere through the effect on a stellar occultation (Millis et al. 1988; Elliot et al. 1989) and the detection of solid N_2 and CO in the near-infrared spectrum, indicating that these molecules must also be major atmospheric constituents (Owen et al. 1993*a*).

II. SPECTROSCOPY OF PLUTO AND CHARON

A. Near-Infrared (1–2.5 μm)

The near-infrared spectral region has proven to be the most diagnostic of the surfaces of Pluto and Charon because ices of the abundant solar system

volatiles have strong absorption bands in this region, and because these bodies are sufficiently bright to allow studies with modern telescopes and spectrometers. This latter fact arises because the Sun provides sufficient illumination and the surfaces are sufficiently high in albedo to give a measurable signal. At longer wavelengths, where even stronger molecular bands occur, the Sun is too faint to give an adequate signal for observations of Pluto and Charon in diffusely reflected light with existing instrumentation. At shorter wavelengths than about 1 μm, the information content of the spectrum appears to diminish because of the decreased strengths of the higher-order overtone/combination vibrations of expected molecules. Thus, the region 1 to 2.5 μm is optimum for measurement of the molecular composition of Pluto's surface, and it is in this spectral interval that all of the molecules found so far have been discovered.

Some of the historical development of spectroscopy of Pluto was noted in Sec. I, and other aspects have been reviewed by Cruikshank and Brown (1986), Clark et al. (1986), Roush et al. (1995), Grundy (1995), and in the chapter by Marcialis. Here we concentrate on the newest results and the summation of our understanding of the surfaces of Pluto and Charon from the spectroscopic viewpoint.

1. Pluto. While CH_4 is the most spectroscopically active molecule found in Pluto's spectrum, the detection of N_2 at 2.148 μm, which has an absorption coefficient $\sim 10^5$ less than CH_4, demonstrated that molecular nitrogen is the dominant ice on the planet's surface (Owen et al. 1993*a*). Frozen CO is also found in Pluto's spectrum as a trace constituent, and most recently, H_2O ice has been found on a portion of the planet's surface (Owen et al. 1996). The absorption bands corresponding to the identified ices are shown on the spectrum of Pluto in Fig. 1. This spectrum is shown in geometric albedo (see caption) for the hemisphere of Pluto corresponding closely to the minimum in the lightcurve (sub-Earth longitude 90 deg), with the contribution of Charon removed. The light from Charon was removed by use of a Hapke spectral reflectance model fit to the data of Buie et al. (1987) (1.5–2.5 μm), recalibrated by Roush et al. (1996), plus the shorter wavelength data of Fink and DiSanti (1988) (see Sec. II.A.2). The individual points in Fig. 1 correspond to the geometric albedo of Pluto near lightcurve maximum (at sub-Earth longitude 180 deg).

The quantitative analysis of Pluto's spectrum, as described in Sec. III, shows by means of scattering models of the planet's spectral reflectance that both CH_4 and CO are minor components (<2% by mass) of the surface materials.

Several important issues have emerged from the quantitative modeling of the spectra of Pluto and Triton (Cruikshank et al. 1993). The first concerns the state of the CH_4 absorption bands. Seen at spectral resolution $R = \lambda/\Delta\lambda = 350$ (0.0063 μm, or 13 cm^{-1}), the CH_4 bands in Pluto's spectrum are shifted toward shorter wavelengths by as much as 0.02 μm, compared to their central wavelengths determined from pure CH_4 in the laboratory. This shift, discovered by Schmitt and Quirico (1992), occurs when CH_4 is dissolved

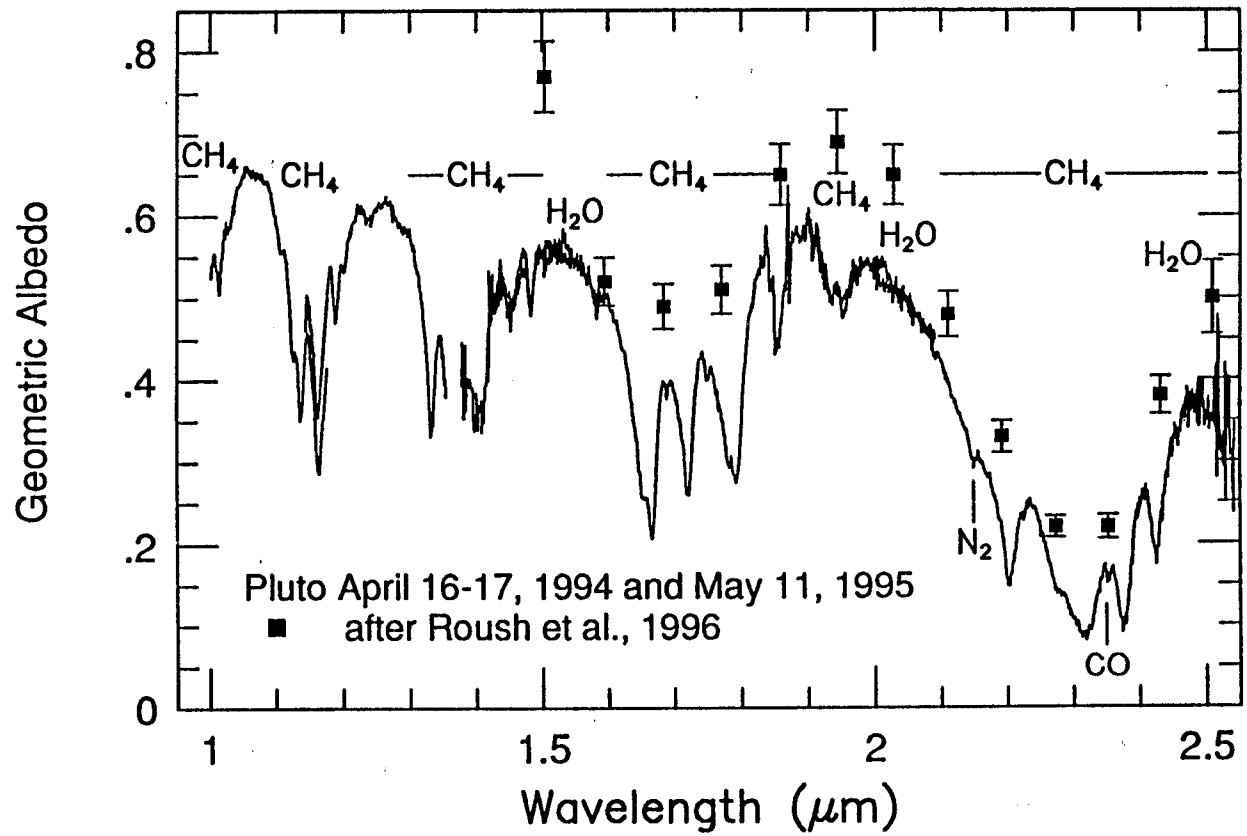

Figure 1. The near-infrared spectrum of Pluto, derived from observations by Owen et al. (1993*a*) and improved data obtained in 1994 and 1995 by the same authors. While the original data include both the light of Pluto and Charon, the contribution of Charon has been removed according to the model discussed in the text. Various portions of the spectrum were observed on different nights and the composite spectrum was assembled by adjusting the intensity calibration of some of the segments to make a more nearly seamless fit; the spectral region 1 to 1.5 μm was adopted as the photometric standard and the spectrum longward of 1.5 μm was adjusted to fit in the region of wavelength overlap. The principal ice absorption bands are identified with the molecular symbol. The symbol H_2O near 2.4 μm refers to the wing of the band centered at longer wavelength. All the data used in this composite were obtained at or near Pluto's lightcurve *minimum*. The geometric albedo was calculated using Pluto and Charon radii of 1150 and 593 km, respectively, and the solar flux given by Smith and Gottlieb (1974). The solid points represent the derived geometric albedo of Pluto near the *maximum* in the lightcurve, using the Roush et al. (1996) recalibration of the Buie et al. (1987) spectrophotometry of Charon.

at low concentrations (~1 molar percent) in a matrix of solid N_2 (see also Cruikshank et al. 1993), and the magnitude of the shift varies from one CH_4 band to another.

Seen at higher spectral resolution (>800), the complex structure of the CH_4 bands indicates that there are two components contributing to the absorption. One component is formed by CH_4 dissolved in N_2, with shifted wavelengths as described above, and another arising from pure CH_4 without the wavelength shifts. The implications of this dual reservoir of CH_4 on the surface structure of Pluto have been addressed by Schmitt et al. (1994); the full implications on the planet's atmosphere remain to be explored fully (see Young et al. 1996).

Solid CO is identified on Pluto by the detection of the (1–0) band at 2.352 μm (and the weaker (2–0) band at 1.578 μm). When CO is dissolved in solid N_2, a wavelength shift of ~0.0006 μm occurs in the 2.352 μm band; this shift is too small to be resolved in existing spectra of Pluto (or Triton). Therefore, it is unclear whether the CO on Pluto is dissolved in N_2 or occurs in independent grains on the planet's surface, although the near complete miscibility suggests the former.

Another factor influencing the models is the state and the temperature of the N_2 giving rise to the absorption band at 2.148 μm. At low pressure, N_2 exists in two distinct phases; above the transition temperature of 35.6 K (for pure N_2), it occurs in a hexagonal phase denoted β. Below that temperature, a higher density cubic α phase exists (Scott 1976). The fundamental absorption band in the spectrum of α-N_2 is characterized by a very narrow phonon absorption band at 4.295 μm superimposed on a broad weaker absorption (Löwen et al. 1990). This band is not observable on Pluto with current technology, but the spectral region of the two-phonon band at 2.148 μm (Grundy et al. 1993) is observable. In the β-phase the N_2 band is shallow and broad, with the absorption peak also at 2.148 μm. In β-N_2 in the temperature range $35.6 \leq T \lesssim 45$ K an additional component appears in the absorption band at 2.160 μm. As Tryka et al. (1993,1995), Grundy et al. (1993), and Grundy (1995) have shown, the shape and strength of this component of the band is temperature sensitive; Tryka et al. (1993, 1994) have used the profile of the β-N_2 band and the 2.160-μm component to establish the temperature of the N_2 on Triton as 38(±1) K and on Pluto as 40(±2) K on the basis of laboratory calibration spectra. The temperature of Pluto is discussed further in Sec. V.

Both CH_4 and CO dissolved in N_2 affect the α-β phase transition temperature, and possibly the appearance of the temperature-sensitive 2.160 μm component of the N_2 band, but at the concentrations of these two molecules estimated on Pluto, the effect on the phase transition temperature is expected to be very small (Scott 1976).

The spectral signature of solid H_2O was first clearly seen on Pluto's surface in data obtained in 1995 (Owen et al. 1996), although the planet's mean density presaged its presence, at least in the subsurface. Water ice behaves as bedrock at the low temperature of Pluto, and as a mixture with

rocky material it provides the planet with its bulk strength and ability to support surface topography (chapter by McKinnon et al.).

In Sec. III we discuss the limitations of the present models of Pluto's surface composition imposed by uncertainties in the nature of the scattering surface and the optical properties of various mixtures of ices of the molecules detected.

In order of decreasing volatility (vapor pressure over the ice at a given temperature), the known molecular components of Pluto's surface are N_2, CO, CH_4, and H_2O. As the most volatile, N_2 contributes most to the planet's lower atmosphere. At T = 40 K (see Sec. V), the vapor pressure of N_2 gas over the pure solid is 58 μbar. To illustrate the steep dependence of the N_2 vapor pressure on temperature, we note that at the extremes of the uncertainty of $\pm$2 K in Pluto's N_2 temperature the vapor pressure is 19 μbar at 38 K and 159 μbar at 42 K (calculated from Brown and Ziegler 1979). It is clear that N_2 dominates the refracting atmosphere discovered in the stellar occultation of 1988 (Elliot et al. 1989).

In addition to these known constituents, systematic searches have been carried out to find other possible ices on Pluto's surface. No evidence of HCN, C_2H_4, C_2H_6 or CO_2 has been found, with upper limits for HCN and the hydrocarbons of approximately 10^{-5} to 10^{-6} relative to N_2 (Owen et al. 1993*a*; Bohn et al. 1994). There are some weak spectral bands that are not yet identified, thus leaving open the possibility that some more complex hydrocarbons may be present (see, e.g., Bohn et al. 1994). Certainly the existence of dark material on Pluto's surface, well demonstrated by the lightcurve and even mapped by the observations of Charon's eclipses and transits (Buie et al. 1992; Young and Binzel 1993), is consistent with *in-situ* chemical reactions that produce additional compounds. On the other hand, this dark material may be exogenous, the residue or product of collisions with dark-crusted comets or carbon-rich icy planetesimals.

Finally, we mention two cosmically abundant substances that are undetectable in this wavelength range, neon and argon. Neon has essentially the same cosmic abundance as nitrogen and a much higher vapor pressure. Thus one might expect it to dominate Pluto's atmosphere. The fact that it does not is consistent with the difficulty in trapping neon in ice that forms at T>25 K. Evidently the ices that formed Pluto, including any late cometary bombardment, were formed at higher temperatures (Owen et al. 1993*a*). Argon is 16 times less abundant than N_2, but could conceivably be enriched on Pluto's surface if nitrogen is readily lost to space. A search for an enrichment of $^{15}N/^{14}N$ on Pluto would test the enrichment scenario; experiments could also be performed to examine the spectrum of a solid solution of Ar in N_2 to see if there are any effects on the N_2 absorption at 2.148 μm.

2. *Charon.* Total eclipses of Charon by Pluto that occurred during the period of mutual transits and eclipses in the 1980s offered opportunities to determine the spectral reflectance properties of Charon, despite the fact that in those days the planet and satellite could not be resolved separately in the

beams of optical telescopes on Earth. Just prior to the first contact of an eclipse of Charon, the optically mixed spectrum of (Charon + Pluto) could be observed. After second contact but before third contact (Charon at superior conjunction, invisible behind Pluto) the spectrum of Pluto alone could be measured, and the difference between the two yields the spectrum of Charon.

Marcialis et al. (1987) made such observations during the eclipse of 3 March 1987 at four discrete wavelengths, 1.5, 1.75, 2.0, and 2.35 μm. Their observations provided a tentative identification of H_2O ice on Charon through the strategic selection of the chosen wavelengths. Buie et al. (1987) made similar observations during the eclipse of 23 April 1987, using 13 wavelengths evenly spaced in the interval 1.56 to 2.51 μm. Their difference spectrum, recalibrated by Roush et al. (1996), is the basis for the four panels in Fig. 2. In that figure we show a model spectrum of H_2O ice with a neutral absorber, as described below (panel c) and the reflectance spectrum of Ganymede (panel d), as well as a range of models incorporating other molecular components (see the figure caption and discussion below). The characteristic shape of the H_2O ice spectrum is clearly seen in the Charon spectrum, and these data, plus the Marcialis et al. result, provide the basis for the identification of frozen H_2O on the satellite (Buie et al. 1987). The shape of the H_2O spectrum is distinct from that of the solid CH_4 seen on Pluto, so the identification of H_2O as the dominant spectrally active solid on Charon is secure.

The results of Buie et al. (1987) and Marcialis et al. (1987) pertain specifically to the observed hemisphere of Charon centered at longitude 0 deg, that is, the hemisphere permanently directed toward Pluto. In efforts to study the near-infrared color signature of Charon at other longitudes on its surface, Bosh et al. (1992) obtained photometry in the K filter band (centered at 2.2 μm) from images of Pluto and Charon in which the satellite was marginally separated from the planet. They found a large variability of Charon and suggested that the satellite has substantial surface variegation as well as a nonuniform distribution of H_2O ice. Buie and Shriver (1994) obtained images with better spatial resolution in the J (1.25 μm), H (1.65 μm) and K (2.20 μm) filter bands, plus two narrow filters centered at 1.5 μm and 1.75 μm, and did not confirm the large K-band variability reported by Bosh et al. (1992). The Buie and Schriver (1994) results are consistent with a uniform distribution of H_2O ice across Charon's surface. The improved quality of the Buie and Schriver data and the lower-amplitude lightcurve they derive tends to favor their result over that of Bosh et al. (1992), but the issue requires further study with data of yet higher quality.

It is important to establish the distribution of H_2O ice and the material that darkens the surface of Charon in order to understand the satellite, but also to aid in the interpretation of the spectrum of Pluto itself. The near-infrared spectrum of Pluto in which the signatures of other ices are so clearly shown also include the light contributed by Charon, and as noted elsewhere in this chapter, the study of H_2O ice on Pluto depends upon the correct evaluation of the contribution of Charon's light.

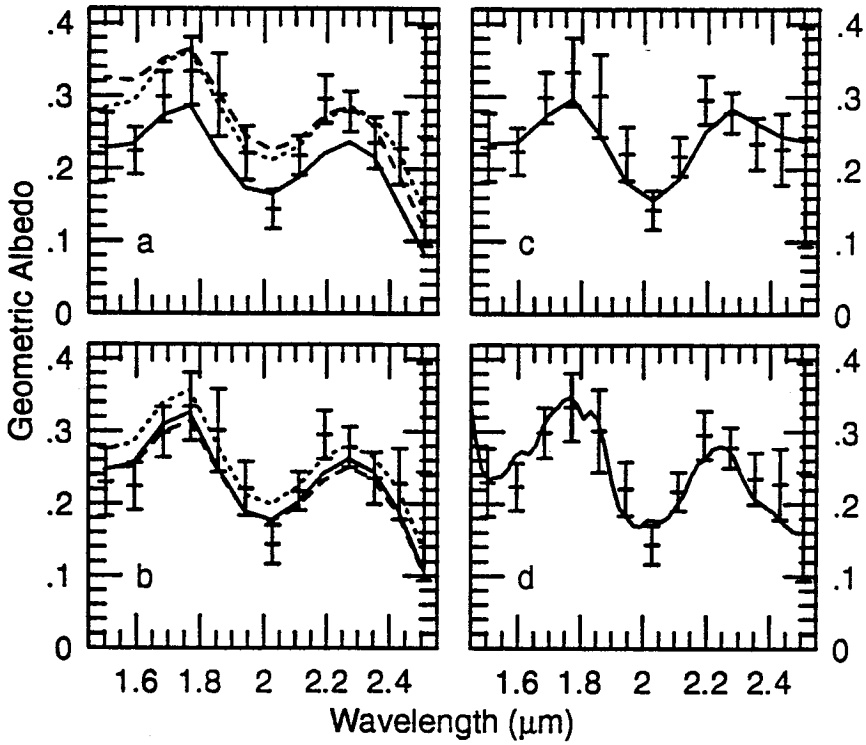

Figure 2. The spectrophotometry of Charon by Buie et al. (1987), shown in geometric albedo as calibrated by Roush et al. (1996) (points with error bars in all four panels). (a) Solid line is a *spatial* mixture of H_2O and CO_2 ices having grain sizes of 200 and 50 μm, respectively, and relative areal coverages of 80% and 20%, respectively. Dotted line is a *spatial* mixture of H_2O and CH_4 ice (grain sizes 50 and 25 μm, and areal coverages of 95% and 5%, respectively). Dashed line is a *spatial* mixture of H_2O, CO_2, and CH_4 (grain sizes 100, 100, and 10 μm, areal coverages of 80%, 19%, and 1%). (b) Charon compared to models of *intimate* mixtures. Solid line is a mixture of H_2O and CO_2 ices (grain sizes 150 and 50 μm and relative mass fractions of 50%). Dotted line is a mixture of H_2O and CH_4 ice (grain sizes 50 μm each, relative mass fractions 50%). Dashed line is a mixture of H_2O, CO_2, and CH_4 ice (grain sizes 100, 100, and 5000 μm and relative mass fractions of 35%, 35%, and 30%, respectively). (c) Solid line is the model described in Sec. II.A.2 of the text. (d) Solid line is the spectral reflectance of Ganymede (leading hemisphere), from Calvin et al. (1995). Panels (a) and (b) are from Roush et al. (1996).

The low-resolution spectrum of Charon by Buie et al. (1987), while diagnostic to first order of the presence of H_2O ice, admits the possibility of other volatiles in significant amounts (Roush 1994; Roush et al. 1996). This basic conclusion is also pertinent to photometry at a smaller number of wavelengths made with broader bandpass filters, such as those of Bosh et al. (1992) and Buie and Schriver (1994). Using the Buie et al. (1987) Charon spectrum and synthetic spectra calculated according to the principles detailed

in Sec. III, Roush found that intimate mixtures of CO_2 and H_2O with as much as 50% mass fraction (relative to H_2O) of CO_2 are consistent with the telescopic data. Smaller amounts of CH_4 ice (depending upon the nature of the mixing and the particle size) could also be "hidden" in the low-resolution Charon spectrum. Roush did not include other plausible volatiles in his models, but by implication, such volatiles as N_2, CO, and various hydrocarbons could be present together with the H_2O in large quantities. The calculations serve to demonstrate that components with absorption spectra weaker than H_2O may occur on Charon in geochemically significant quantities, and models of the chemical history and evolution of the satellite should not be artificially constrained by the apparent surficial dominance of H_2O ice.

Grundy (1995) derived the spectral geometric albedo of Charon from the Buie et al. (1987) data and those of Fink and DiSanti (1988). Grundy found that a scattering model with an intimate mixture of 88% H_2O ice and 12% spectrally neutral absorber (absorption coefficient of 100 cm^{-1} and refractive index 1.3, all with 50 μm grains), provides a satisfactory, but not unique, fit to the data between 0.6 and 2.5 μm.

As already noted, in Fig. 2 we show the reflectance of Charon derived by Roush et al. (1996) from a new calibration of the Buie et al. (1987) data, plus spectra of H_2O ice modeled with a neutral absorber (panel c) and in combination with ices of CH_4 and CO_2. The model in panel c consists of an intimate mixture of 85% H_2O ice plus 15% amorphous carbon, both with 50 μm grains. Optical constants for H_2O ice at 100K were used. The spectral geometrical albedos derived by Roush et al. (1996) with pure H_2O ice are nearly identical to those found by Grundy (1995) in the 1.5 to 2.5 μm region, but when the constraint imposed by the Fink and DiSanti (1888) data in the 0.5 to 1.0 μm region is added, an additional strong absorbing component is required. The Charon model spectrum used to produce the Pluto geometric albedo spectrum in Fig. 1 and panel c of Fig. 2 is the 85% H_2O plus 15% amorphous carbon mixture noted above.

B. Photovisual Spectral Region (0.3–1.0 μm)

1. Pluto. Observations of Pluto in the photovisual spectral region have been obtained by multi-filter photometry and with dispersive spectrometers, most recently using CCD detectors. Figure 3 shows a combination of filter photometry by Bell et al. (1979) and an image-dissector-scanner dispersive spectrum by Barker et al. (1980). Both of these data sets represent the reflectance of Pluto plus Charon. Except for the points in the ultraviolet, the normalized spectra show satisfactory agreement in terms of the slope upward toward longer wavelengths. Spectra obtained one year later by Fink et al. (1980) between 0.6 and 1.0 μm show a somewhat less steep red color for Pluto (plus Charon), and reveal several CH_4 bands (originally attributed entirely to the gaseous atmosphere, but now known to arise primarily from solid methane on the surface). Numerous subsequent spectra of Pluto also show this more modest red slope in the color (see, e.g., Fink and DiSanti

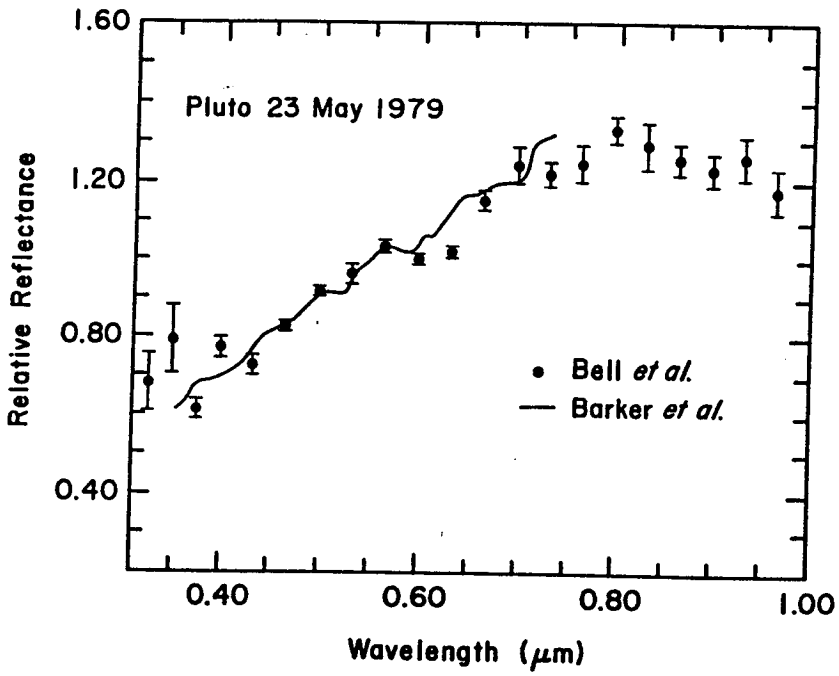

Figure 3. Spectral reflectance of Pluto (including the light of Charon) in the photovisual spectral region. The points are from Bell et al. (1979) and the solid line from Barker et al. (1980) (figure from Cruikshank and Brown 1986).

1988; Marcialis et al. 1992; Grundy 1995).

Buie (1984) and Buie and Fink (1987) obtained spectra of the Pluto–Charon pair with the Fink CCD spectrograph at four different rotational aspects of the system in 1983 April. Reducing the spectra to geometric albedo, they found variations in both albedo and CH_4 band strength that are correlated with rotational phase; the bands appear weakest at Pluto's minimum point in the rotational lightcurve (0.0 rotational phase = 90 deg sub-Earth longitude = Charon's northern elongation).[a] As the authors noted, if the methane were primarily in the atmosphere, the band strengths should be constant (to first order) with the planet's rotation; their observed variation confirmed that the CH_4 bands occur primarily in the solid surface.

Separate spectra of Pluto and Charon were obtained in the region 0.54 to 1.02 μm by Fink and DiSanti (1988) during the eclipse of Charon on 3 March 1987. The spectrum of Pluto alone shows the CH_4 bands seen in 1980,

[a] Pluto's rotational phase is defined as 0.0 at the minimum in the lightcurve, at which time the sub-Earth longitude is 90 deg and Charon is at northern elongation. At the current epoch, Charon then moves to inferior conjunction, southern elongation, and then to superior conjunction, while the sub-Earth longitude on Pluto decreases toward 0 deg, then to 270 deg, 180 deg, etc. The sub-Pluto longitude on Charon is defined as 0 deg.

with possible variations in the strength of the 0.72 μm band. (The sub-Earth longitude of Pluto in the Fink et al. 1980 observations was ~0 deg, while the 1987 data refer to 180 deg [at the time of Charon's superior conjunction].) Small differences in the slope of the spectrum and the CH_4 band strengths are probably the result of the different regions of Pluto viewed; possible changes in Pluto's atmosphere between 1980 and 1987 are expected to make negligible changes in this low-resolution spectrum.

Grundy (1995) modeled the CH_4 bands in Pluto's photovisual spectral region using a Hapke scattering model and a new suite of laboratory data on solid CH_4, particularly CH_4 dissolved in solid N_2, from which the optical constants were derived. This work included the analysis of weak CH_4 bands at 0.73, 0.79, 0.89, 1.0, and 1.15 μm. No frequency shifts were found for CH_4 dissolved in solid N_2 for these bands, nor were there any detected frequency shifts with temperature. Grundy's work expands upon Buie's (1984) scattering models of Pluto's CH_4 bands, which were based on optical constants derived from spectra of liquid CH_4; the spectrum of liquid CH_4 is similar to that of room-temperature gaseous CH_4 when extrapolated to liquid densities (Khare et al. 1990).

Grundy (1995) noted that the weak bands of CH_4 in the photovisual region are enhanced in strength relative to the stronger CH_4 bands, as Owen et al. (1993*a*) had noted at longer wavelengths, and he discussed various possible mechanisms. Among the possible causes of the absorption strength discrepancy noted by Grundy are (1) multiple grain sizes for the CH_4, (2) differing concentrations of CH_4 in N_2 in different regions of the planet's surface, (3) different terrain types having different CH_4 concentrations. These and other possible causes of the band strength differences require further study.

In his study of spectra (0.5–1.0 μm) of Pluto (including the light of Charon) obtained with the same instrument over a span of 12 years (1983–1994), Grundy (1995) considered various spectral parameters as a function of the planet's longitude (lightcurve phase). He found that the CH_4 bands in this spectral region are weakest not at the minimum in the rotational lightcurve (longitude 90 deg), but at ~160 deg, midway on the steep slope between maximum and minimum brightness. Note that this result differs from those of other investigators reported in Sec. I. Grundy was working with the weaker bands in the photovisual region, but had a large number of spectra with good sampling over the entire lightcurve. His results and those in the near infrared showing CH_4 band strengh minimum at Pluto's minimum in the lightcurve require further analysis.

Grundy (1995) also reported a small secular weakening of the 0.73 μm CH_4 band relative to the band at 0.89 μm over a seven-year period. This change may be related to the changing viewing geometry of Pluto's polar regions, or a small change in the N_2 abundance over this time period.

In order to model the spectrum of Pluto (see Sec. III below), the spectral distribution of the geometric albedo must be established. This information has been derived by the subtraction of the contribution of the light of Charon to the

observed light of (Pluto + Charon) by Marcialis et al. (1992), Grundy (1995), and Roush et al. (1996), and in Fig. 1 of this chapter. All three derivations use the Fink and DiSanti (1988) data (0.5–1.0 μm) for Charon from the eclipse of 3 March 1987.

2. *Charon.* Models of the first observations of the mutual eclipses and transits of Pluto and Charon showed that the geometric albedo of Charon is significantly less than that of the average surface unit on Pluto (Tholen et al. 1987). The photometry of the mutual events showed that the depths of the lightcurves of the superior events (Charon behind Pluto) were wavelength dependent, while the depths of the transits (Charon in front of Pluto) were not. Tholen et al. (1987) suggested that Charon had two hemispheres of different color, but additional data by Binzel (1988) and Tholen and Buie (1988) caused the authors to reject this notion in favor of Binzel's (1988) model in which the reflectance of Charon is uniform, with the same color as Pluto's polar caps, and that Pluto's equatorial region is dark and reddish.

Tholen and Buie (1988) derived the *B* albedo (0.47 μm) of Charon as 0.375, while for the eclipsed hemisphere of Pluto the *B* albedo is spatially variable over the range 0.43 to 0.60 (with a spatial scale comparable to the projected size of Charon). Their albedo for Charon is consistent with independent derivations from CCD spectra (Marcialis et al. 1992; Grundy 1995), and with newer calibrations of the near-infrared data (Marcialis et al. 1992; Roush et al. 1996, and the Charon model used in the derivation of Fig. 1 of this chapter).

The photovisual spectrum of Charon derived from observations before and during eclipses by Pluto shows that the satellite has no discernible spectral bands in the region 0.54 to 1.0 μm (Fink and DiSanti 1988). Using the dimensions R = 1145 km for Pluto and R = 642 km for Charon, Fink and DiSanti found that the satellite's albedo gradually and uniformly decreases from 0.36 at 0.55 μm to 0.33 at 1.0 μm (nearly neutral reflectance). The satellite is, therefore, distinctly more neutral than Pluto in this spectral region, as it is in the near-infrared. Furthermore, the near-neutral and featureless reflectance of Charon is consistent with H_2O frost as its major surface component, as established from near-infrared data discussed above.

In subsequent investigations, maps of Charon derived from observations of the mutual transits and eclipses suggest that the satellite is in fact not uniformly reflective (Buie et al. 1992), but the rotational lightcurve of Charon (Olkin et al. 1993) shows a variation of only 0.10±0.07 at the *B* wavelength (0.47 μm). Photometric observations with the Hubble Space Telescope and the Planetary Camera in which the images of Pluto and Charon are clearly separated show no evidence for strong brightness variations as the satellite rotates on its axis. Buie et al. (1994) derived an upper limit of 0.04 stellar magnitudes for the lightcurve amplitude, while the analysis of a different (spectroscopic) data set by Trafton and Stern (1994) gave an unconstraining upper limit of 0.12 mag for Charon's lightcurve at 0.33 μm.

For the calculated models presented here and by Owen et al. (1993*a*),

no surface variegation of Charon is included. Furthermore, there is no information on the composition of the material that causes the overall geometric albedo of the satellite to be lower than that of Pluto, except that it is very likely to be neutral in color over the wavelength range 0.4 to 2.5 μm. Amorphous carbon and graphite are neutral absorbers that meet this requirement, while most silicates and refractory organic solids are expected to alter the neutral color of Charon.

C. Ultraviolet (<0.3 μm)

1. Pluto. Spectra of the Pluto–Charon system with the International Ultraviolet Explorer (IUE) satellite were used by Stern et al. (1991) to determine the albedo of the combination of the two bodies between 0.255 and 0.320 μm, and to show albedo changes during the rotation period. No spectral absorption features were detected. The ultraviolet spectrum has not yet yielded new information about the surface composition, but improved data from the Hubble Space Telescope may bear on this matter.

2. Charon. We await HST data on Charon resolved from Pluto for any insight that may be gained from the ultraviolet spectrum.

III. MODELING THE REFLECTANCE SPECTRA OF PLUTO AND CHARON

A. Types of Mixtures

To model the reflectance spectrum of an object the mixing nature of the various surface components must be considered. Here molecular, intimate, and spatial mixtures are considered in order to include potential mixing of components at a variety of scales. Molecular mixtures describe mixing that occurs while the individual components (e.g., N_2, CH_4, etc.) are gases which subsequently condense. The resultant solid is a material with mixing occurring at molecular dimensions. Depending upon the relative abundance and compositions of the components, this mechanism can result in solid solutions, where one component substitutes within the crystal structure of the other, or alternatively matrix isolation, where one component occurs as an isolated molecule trapped in the structural matrix of the other component(s). As an alternative, intimate mixtures describe the situation where discrete grains of pure materials have condensed separately but the resulting solids have been subsequently mixed together at the granular (micrometer to millimeter) scale. Terrestrial soils or the lunar regolith are examples of intimate mixtures. As a third alternative, spatial mixtures describe mixing of pure materials at macroscopic scales (e.g., checker-board mixing), such as individual outcrops or regions of pure materials.

B. Mathematical Modeling

1. Molecular Mixtures. Mathematical models for calculating the reflectance spectra of surfaces composed of molecular mixtures from the optical prop-

erties of the individual components do not exist. The optical properties of the individual components only serve as a guide to the spectral regions where features may be anticipated. However, it is known that matrix isolation produces significant shifts in both the positions and intensities of absorption features (see, e.g., Van Thiel et al. 1957; Allamandola 1984; Schmitt et al. 1993). For modeling purposes, the optical properties must be determined from the molecular mixtures and then used to calculate the reflectance for either an intimate or spatial mixture that contains the molecular mixture as one or more components.

2. *Intimate Mixtures: Equations and Assumptions.* Hapke (1981,1984, 1986,1993*a*,*b*) has developed a series of equations, based on a two-stream approximation to the equations of radiative transfer, that provide the ability to calculate the reflectance of intimate mixtures, given assumptions or knowledge of the physical nature of solid phases comprising the surface. The bidirectional reflectance of a surface, at each wavelength (λ), can be expressed as

$$r(i, e, g, \overline{w}, h, S(0)) = \frac{\overline{w}}{4\pi} \frac{\mu_o}{\mu_o + \mu} \{[1 + B(g)]P(g) + H(\mu)H(\mu_o) - 1\} \quad (1)$$

where i is the angle of the incident light ($\mu_o = \cos i$), e is the angle of the emergent light ($\mu = \cos e$), g is the phase angle between i and e, $\overline{w}$ is the average single scattering albedo of the particles composing the surface, h characterizes the width of the opposition surge in terms of the microstructure of the surface (porosity, particle size distribution, and compaction rate with depth), $S(0)$ is the opposition surge amplitude and characterizes the contribution of light scattered from near the front surface of individual particles at zero phase. The opposition surge is expressed as

$$B(g) = \frac{B_o}{1 + \frac{\tan(g/2)}{h}} \quad (2)$$

where

$$B_o = \frac{S(0)}{\overline{w}P(g=0)}. \quad (3)$$

For icy surfaces, at visual wavelengths, the parameter h varies from a low of ~0.018 for Europa, Titania, and Oberon (Domingue et al. 1991; Verbiscer and Ververka 1989; Helfenstein et al. 1988) to roughly 0.07 for Umbriel, Mimas, and Rhea (Helfenstein et al. 1988; Verbiscer and Ververka 1989,1992). In the near-infrared (1.0–2.5 μm) h has not yet been reported for icy surfaces. Here we assume $h = 0.05$ and $S(0) = 1.0$. In all of the models we assume an isotropic phase function, implying a maximum geometric albedo of approximately 0.7 (Hapke 1984). $H(\mu_o)$ and $H(\mu)$ are Chandrasekhar's H-functions (1960). From Eq. (17) of Hapke (1981), the average single-scattering albedo is

$$\overline{w} = \frac{\sum_{i=1}^{n} \frac{M_i}{\rho_i D_i} Q_{Si}}{\sum_{i=1}^{n} \frac{M_i}{\rho_i D_i}} \quad (4)$$

where M_i, ρ_i, and D_i are the mass fraction, solid density, and diameter of the ith particle, respectively. The scattering efficiency of the ith particle (Q_{Si}) is related to the volume absorption (α) and scattering (s) coefficients inside the particle (Hapke 1984). The imaginary index of refraction (k) is related to α via the dispersion relation ($\alpha = 4\pi k/\lambda$). In all the models we assume minimal internal scattering, and hence let $s = 10^{-17}$. Parameter $\overline{w}$ in Eq. (4) contains direct compositional information because the indices of refraction are wavelength dependent.

3. Spatial Mixtures. For spatial mixtures, the reflectances of the individual components (which may themselves be intimate mixtures) are calculated using Eqs. (1–4) above. These reflectances are then combined at each wavelength to represent the total reflectance (R_T) of a spatial mixture via:

$$R_T = (A * R_A) + (B * R_B) + \cdots + (N * R_N) \quad (5)$$

where R_A, R_B, and R_N are the reflectances and A, B, and N represent the areal extent or spatial coverage of each component such that they sum to 1.0, respectively.

C. Optical Constants

1. Molecular Mixtures. The real (n) and imaginary (k) indices of refraction of molecular mixtures must be determined on a mixture-by-mixture basis. While these values are available in the mid- and far-infrared for a variety of mixtures (see, e.g., Hudgins et al. 1993), their availability in the near-infrared is extremely limited (B. Schmitt, personal communication 1992; D. Hudgins, personal communication 1991). As a result, we have not modeled such mixtures, even though it appears that CH_4 is dissolved in N_2 on both Pluto (Owen et al. 1993*a*) and Triton (Cruikshank et al. 1993). For the calculations performed here we have represented the optical constants of CH_4:N_2 molecular mixtures by shifting the wavelengths of the peak k values of pure CH_4 those corresponding to the shift observed in the Pluto data (see Sec. II.A.1 above).

2. Intimate and Spatial Mixtures. The real and imaginary indices of refraction for the various ices used in these calculations are obtained from a variety of sources. Values for H_2O ice are taken from Warren (1984) and Roush (1996). The values for both CO and CH_4 ice were provided by Bernard Schmitt (Schmitt et al. 1992), and the values for β-N_2 were provided by R. H. Brown (Green et al. 1991). These refractive indices were convolved to the same resolution as the observational data using a Gaussian to represent the bandpass of the spectrometer.

3. Caveats. As outlined in the equations above, the calculated reflectances are directly influenced by any changes in the optical constants used in a calculation. If the optical constants are revised or supplanted by newer more accurate values, then the results and conclusions presented here should be reviewed. Additionally, if the optical constants were determined for ices

at a temperature significantly different from that of Pluto (~30–45 K) and if the optical constants are temperature-dependent (see, e.g., Grundy et al. 1993; Schmitt et al. 1993,1994) then the discussions and conclusions below may be influenced accordingly.

D. Results of the Models and Compositional Implications

To reiterate briefly the discussion in Sec. II.A, the 1.2- to 2.4-μm high resolution spectra of Pluto exhibit absorption features due to CH_4, CO, and N_2 ices. The relatively low resolution spectrum of Charon (Buie et al. 1987) exhibits absorption features consistent with the presence of H_2O ice, although a variety of other volatile ices can not be excluded by these same data (Roush 1994). Beginning with this knowledge the high resolution spectra of Pluto are modeled. The modeling reported by Owen et al. (1993*a*) consisted of an empirical, but not exhaustive, search of the relevant parameter space of relative mass fraction and grain size of each component. In general, the grain sizes and relative abundances discussed below are probably accurate to a factor of two. See Table I.

1. Intimate Mixtures. The Pluto spectrum was modeled by representing the entire surface as being homogeneously covered by an intimate mixture consisting of CH_4, CO, and N_2 ices. Similarly, the surface of Charon was represented as pure H_2O ice grains of diameter 75 μm using optical constants from Wareen (1984). Subsequent models should use an intimate mixture of H_2O ice plus a neutral absorber, as described in Sec. II.A.2 and optical constants for ice of the appropriate temperature and phase. Assuming a grain diameter and relative abundance for each component, the reflectance of the mixture representing Pluto was calculated. Subsequently, this result was combined with the reflectance representing Charon by weighting the relative contribution of each body to the observed spectrum by each body's projected area (Pluto = 73.4% and Charon = 26.6%), in a manner equivalent to the mixing described by Eq. (5) above. In calculating the projected area, the radii of Pluto and Charon used were 1150±7and 593±10 km, respectively (Buie et al. 1992).

Initially, both the models and the observational data were divided by a continuum to allow for intercomparisons (Owen et al. 1993*a*). By varying the particle diameters and relative abundances of the individual components representing Pluto, the effects on the resultant reflectances were investigated until a model that remained consistent with the observational data was determined. It was found that large grain diameters and abundances of N_2 were required to reproduce the observed N_2 absorption band, appearing as a shoulder at 2.15 μm in the observational data. In addition, the presence of fine grained (tens of micrometers) CO or CH_4 ices begin to mask the N_2 band at relatively low abundances. The mixture shown by Owen et al. (1993*a*) provided a reasonable correspondence to the observational data, but not an exact fit. In particular, the CH_4 band depths in the 1.7 μm region and near 2.2μm are slightly too deep, while at the same time the 2.3 μm band is too weak but

TABLE I
Model Abundances for Pluto, Charon, and Triton

	Pluto		Charon		Triton	
Ice	Abundance	Grain Size	Abundance	Grain Size	Abundance	Grain Size
N_2	98%	10 mm	—	—	99.75%	8 mm
CO	0.5%	0.5 mm	—	—	0.1%	1 mm
CH_4	1.5%	[0.25 mm]	—	—	0.05%	[0.2 mm]
CO_2		—	—	—	0.1%	0.8 mm
H_2O	?	?	50–100%	0.05–0.1 mm	?	?

the 2.37 μm band matches the data quite well. Additionally, two weak CH_4 bands at 1.58 and 1.74 μm present in the model calculation are not observed in the telescopic data. The observed N_2 band is approximately reproduced by the model. The discrepancy between the observations and the model in the 1.45 to 1.6 μm region is a result of absorption by H_2O ice, perhaps suggesting too great of a contribution ascribed to Charon, or alternatively, it may be H_2O ice on Pluto (Owen et al. 1996) that was not included in the modeling.

In an attempt to retain absolute albedo information, the geometric albedo (ρ_λ) was calculated via

$$\rho_\lambda = \frac{R^2 d^2}{r^2} \frac{\mathcal{F}_P}{\mathcal{F}_\odot} \tag{6}$$

where R is the heliocentric distance, d the geocentric distance, r the radius of Pluto, $\mathcal{F}_P$, is the flux from Pluto, and $\mathcal{F}_\odot$, is the solar flux calculated from the expression of Smith and Gottlieb (1974). The results of this calculation are shown in Fig. 4 for the 1992 data. The absolute albedo level for the two wavelength regions may differ because they were acquired on two different days and hence sampled different regions on Pluto and Charon. The Owen et al. (1993*a*) model mixture was used to calculate ρ_λ by performing an 8 point Gaussian quadrature for i and e similar to that described in Roush et al. (1990); the results are shown in Fig. 4. The overall shape of the model spectrum remains fairly consistent with the observational data but the overall albedo level appears to be slightly too high.

2. *Spatial Mixtures.* A more complex model, representing Pluto's surface as having two spatial components, is now considered. One component is an intimate mixture of N_2, CO, and CH_4 ices and the other is a pure CH_4 frost. This consideration is based upon the width and wavelength shift observed in Pluto's CH_4 absorptions. The wavelength shift is attributed to CH_4 dissolved in N_2, while the width arises from the overlapping absorptions of pure CH_4 and those due to CH_4 in N_2. The result for a spatial extent of 20% CH_4 frost is shown in Fig. 5. No specific effort was made to optimize a solution for relative spatial coverage or grain size of the pure CH_4. Nevertheless, this mixture compares quite well with the observational data with the exception of the 2-μm region. For this grain size and abundance the CH_4 bands near 1.65 and 2.2 μm are becoming too strong, suggesting that in this case 20% spatial coverage of CH_4 represents an upper limit. A different abundance or grain size of pure CH_4 could provide a better match.

E. Summary of Model Calculations

The results of the calculations presented here indicate that the high-albedo surface units of Pluto are dominated by an intimate mixture of N_2, CO, and CH_4 ices. The calculations made to date suggest that these high-albedo units comprise roughly 80% of the surface, but surface temperature considerations (see Sec. V) may not be fully compatible with such a large area of high albedo. Within this mixture N_2 ice is the most abundant component at ~98% while CO

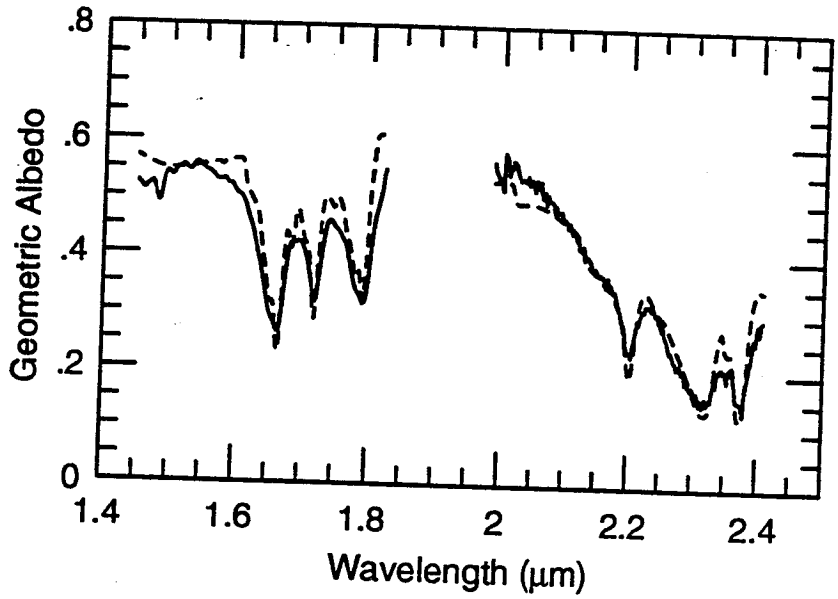

Figure 4. The geometric albedo of Pluto derived from the 1992 observations (solid line) compared to the geometric albedo calculated using the mixture of Owen et al. (1993*a*) (dashed line). The mixture of Owen et al. (1993*a*) consists of 98% N_2 ice, 1.5% CH_4 ice, and 0.5% CO ice with grain diameters of 1 cm, 0.25 mm, and 0.50 mm, respectively, representing the surface of Pluto and H_2O ice with a grain diameter of 0.075 mm to represent Charon.

and CH_4 are relatively minor components at ~0.8% and 1.2%, respectively (all fractions are mass fractions). The other regions on Pluto may contain pure CH_4 ice at ~20% of the surface area, although more specific constraints await further modeling.

F. Improving the Models

As more observational data become available, at near-infrared and other wavelengths (e.g., Fig. 1), it is imperative to the modeling effort that appropriate and accurate optical constants are available. For example, recent laboratory measurements by Schmitt et al. (1992), Grundy et al. (1996), and Quirico and Schmitt (1996) are providing information for CH_4 in the 0.68 to 3.3 μm region that will be useful in modeling historic (Grundy and Fink 1993) and continuing observations of Pluto (Owen et al. 1993*b*). Schmitt et al. (1993,1994) and Grundy et al. (1996) are investigating the effects of temperature, concentration of CH_4, and crystallization history on the optical properties of N_2:CH_4 molecular mixtures that will be useful in future modeling. The optical constants of water ice measured at appropriate low temperatures could also improve the modeling efforts. Consideration of anisotropic scattering or grain size distributions of the components may provide a means of reducing some of the remaining discrepancy between the models and observational data. However,

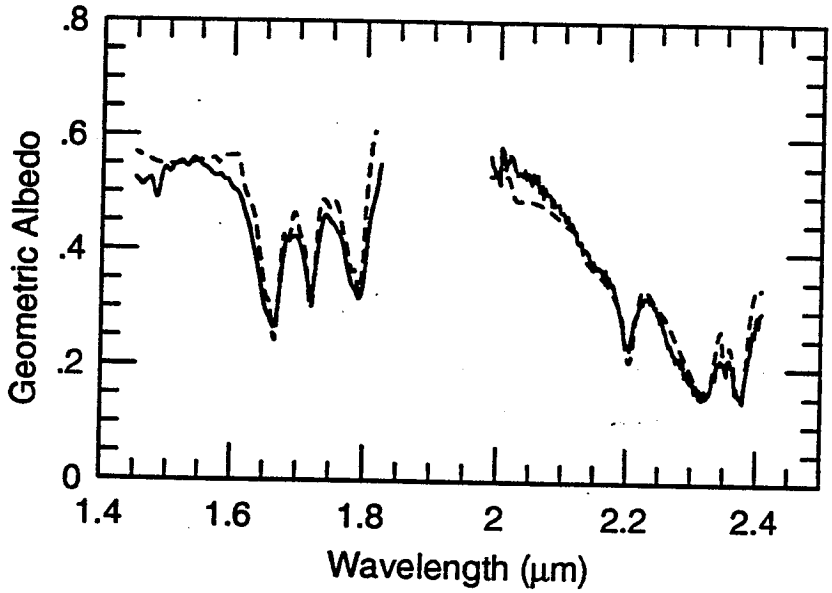

Figure 5. The 1992 geometric albedo of Pluto (solid line) compared to the geometric albedo calculated for a mixture that includes a component of pure CH_4 ice on Pluto (dashed line). The mixture representing Pluto now consists of two spatial components. One component covers 80% of the surface area of Pluto and is composed of 98% N_2 ice, 1.2% CH_4 ice, and 0.8% CO ice with grain diameters of 1 cm, 0.40 mm, and 0.30 mm, respectively. The other component covers 20% of Pluto's surface and is pure CH_4 ice having a grain diameter of 0.25 mm.

care must be taken to ensure that observations of Pluto at all wavelengths are directly comparable and not sampling different portions of the rotational phase curve. Even then, retaining absolute albedo information requires more specific knowledge regarding the relative contribution of Charon. Ideally, separate spectra of Pluto and Charon should be obtained simultaneously over the entire wavelength region of interest.

IV. SURFACE MICROSTRUCTURE

A. Pluto

Solid nitrogen has a very weak spectral absorption coefficient. Therefore, the presence of the 2.148 μm absorption band indicates that photons from the Sun must traverse several centimeters of transparent N_2 ice before they are scattered back to the observer on Earth. Such a long pathlength is counter-intuitive because of the common experience of viewing a snow-covered terrestrial surface in which the optical pathlength is only a few mm. A more relevant common experience is that of viewing a patch of very clear ice on a frozen pond through which only a few random cracks interrupt the view to a depth of a few tens of cm. The portions of Pluto's surface covered by N_2 must have a

surface microstructure that permits optical penetration to considerable depth in order to produce the spectral absorption band observed. That is to say that the surface is locally smooth on cm scales, and scattering centers, which may be grain boundaries, cracks, or bubbles, are very sparse in Pluto's N_2 ice.

The structure of Pluto's icy surface must be similar in many ways to that of Triton, whose surface also has large regions covered with transparent solid N_2 with minor amounts of CO and CH_4 (plus exposures of solid CO_2) (Cruikshank et al. 1993). Eluszciewicz (1991; see also Brown et al. 1995) explored the microstructure of Triton's N_2-rich surface, finding that solid N_2 can form a polycrystalline layer with few scattering centers. Similar processes will likely occur on Pluto.

Details of the seasonal condensation-evaporation cycle for the volatiles on Pluto are unknown (see the chapter by Spencer et al.), but there is every expectation that at least a portion of the N_2 inventory is evaporated from some regions of the surface and deposited elsewhere during the seasonal cycle. Freshly deposited N_2 probably occurs in fine crystals, which are then sintered to form a highly transparent polycrystalline structure with very few scattering centers. Because N_2 gas dominates the atmosphere, the solid frost tends to condense without bubbles of impurity gases; the CH_4 detected in the atmosphere and in the ice, and the CO detected in the ice, are both soluble in N_2 in a solid solution, and are presumed to co-condense with the N_2, at least in part. Their solubility helps ensure against formation of CH_4 and CO bubbles. The polycrystalline N_2 layer might crack during seasonal temperature changes, particularly if the N_2 is cycled between the α and β phases where a volume change occurs (Duxbury and Brown 1993). At most times, however, N_2 at the surface is held at a uniform temperature throughout the diurnal cycle by latent heat "clamping"; the temperature at depth can vary on a seasonal, but probably not diurnal, cycle.

Eluszciewicz (1991) and Brown et al. (1995) have described the sintering process in which individual grains or polycrystals fuse into a large-scale transparent volume. As adjacent contacting grains strive to minimize surface energy, in a way similar to fusing water drops, the contact points slowly enlarge, moving the grain centers closer to one another, eventually resulting in larger grains, lesser interstitial volume, and increased bulk density. Eluszciewicz (1991) discussed the known mechanisms contributing to sintering, concluding that grain boundary diffusion and lattice diffusion from boundary sources dominate the metamorphosis of N_2 grains on Triton.

Time scales for the grain growth and densification scale roughly with the third or fourth power of the grain size. Eluszciewicz (1991) found for the N_2 on Triton that the densification time scale only becomes shorter than a season for grains smaller than 10 to 30 μm. Thus, deposits (condensates) less than this size sinter to form a continuous sheet of N_2 in one season, but substantially larger particles (such as the 100 μm particles that may constitute the equatorial blue collar of Triton [Yelle et al. 1991]) will remain as a highly

scattering particulate surface for a very long time.[b] The seasonal cycle of Pluto (~62 yr) is longer than that of Triton (40.5 yr), so grain growth to 100 μm dimensions may not be unexpected there. Polycrystalline grains are inefficient scatterers because there is no change of refractive index across the grain boundaries, whereas bubbles or cracks will scatter efficiently. Therefore, the condition of large optical pathlength in solid N_2 is met for a densified surface with a small residual number of scattering centers.

The microphysical state of Pluto's surface at the current epoch (~1 decade past perihelion) is not uniform, as indicated by the albedo distribution shown in maps at various colors and as implied by the nonuniform temperature distribution (see Sec. V). Nitrogen ice is probably absent at the equator, where dark material of unknown composition and structure occurs at a temperature that is likely too high for N_2 condensation or retention.

B. Charon

The only spectroscopically identified component of Charon's surface is solid H_2O, as discussed in Sec. II.A.2, although there is evidence from the relatively low albedo and its nonuniform distribution that at least one additional component is mixed with the ice. This additional material appears to be spectrally neutral. The initial comparison of Charon's surface with that of H_2O frost (Buie et al. 1987), and the later models by Roush (1994) and Roush et al. (1996) show that grain sizes of ~75 to 150 μm match the band strengths between 1 and 2.5 μm wavelength.

At the temperature of Charon, H_2O grain sintering proceeds at a negligible rate. The extremely low vapor pressure also precludes significant grain growth by evaporation and local condensation in the manner described by Clark et al. (1983). In addition, there is no evidence for large-scale seasonal or secular evaporation and condensation of H_2O on the surface. Consequently, the ice on Charon is probably an ancient deposit having a granular surface that is altered only by space weathering processes and impact gardening. (The possibility that the solid-state greenhouse effect might raise temperatures in the H_2O ice sufficiently to induce ice-grain metamorphosis remains to be evaluated.) *A priori*, we might expect the surface of Charon to be darker than that of Pluto, because the latter can be refreshed by the seasonal transport of nitrogen, while the former evidently cannot. However, if the surface of Charon is really dominated by H_2O ice, then Pluto obviously has more potential to produce dark material from its surface by irradiation of CH_4. Hence an accurate determination of Charon's surface composition assumes additional importance. In the absence of a darkening component, Charon's surface would be highly backscattering and would have a high albedo. The

[b] Little N_2 absorption occurs in grains smaller than a few mm. Therefore, the observed N_2 band in Triton's spectrum must arise mostly from areas of the satellite's surface covered with cm-size grains. Reflectance from those regions of Triton covered by much smaller grains will slightly dilute the N_2 band with diffuse continuum radiation.

darkening of the surface may have occurred through irradiation processes in the ice, by impact excavation of rocky material from the subsurface, by the deposition of material from external sources, or by some combination of these processes.

V. TEMPERATURES ON PLUTO

A. Indirect Techniques

The diverse information about Pluto gathered from spectroscopy, radiometry, photometry, and particularly analysis of data from the mutual transits and eclipses with Charon, has given us both direct and indirect information about the planet's temperature. The emerging picture is one of a complex surface temperature distribution which changes with time and drives annual variations in atmospheric column density, as well as changes in the surface composition and the distribution of bright volatile ices over portions of a surface that may otherwise have a low albedo. To understand this temperature distribution requires an examination of the full range of data in a process much like assembling a puzzle, each piece of which conveys only part of the total picture.

Temperature values for Pluto have been inferred from the detections of surface ices and an atmosphere, and they have been derived from models of the directly detected thermal radiation from the planet and its moon. When methane frost was first detected (Cruikshank et al. 1976) followed by a report of methane gas (Fink et al. 1980), an attempt was made to constrain Pluto's surface temperature by presuming the ice to be isotropically distributed and requiring the vapor pressure of the gas phase to support the atmosphere (Trafton and Stern 1983). The result was a globally isothermal surface temperature of 59 K, which is above the ~43 K blackbody temperature expected for an object at Pluto's heliocentric distance, and was explained by positing a very low thermal emissivity for methane ice. The original report of a substantial CH_4 atmosphere was incorrect because Fink et al. (1980) attributed all of the absorption they observed to the gas, whereas solid CH_4 accounts for the great majority of the absorption in the bands (Cruikshank and Silvaggio 1980; Buie 1984) throughout the spectrum. Thus, there was never any true spectroscopic evidence for a dense CH_4 atmosphere, high surface temperature, or low CH_4 emissivity.

The discovery of Pluto's atmosphere by observations of the stellar occultation of 1988 (Millis et al. 1988; Elliot et al. 1989) demonstrated the presence of a gaseous component other than CH_4 (Hubbard et al. 1988; Yelle and Lunine 1989; Stansberry et al. 1994), and when Owen et al. (1993*a*) discovered solid N_2 on Pluto, that component was established as nitrogen. The surface temperature required to produce the partial pressure of nitrogen needed to support the atmosphere was estimated at 35 K (Owen et al. 1993a; Stern et al. 1993). The temperature of the surface supply of N_2 to the atmosphere was tightly constrained by this reasoning, because the very strong

relationship of vapor pressure to temperature results in a factor of 10 difference in atmospheric surface pressure for a temperature difference of only 4.25 K. However, the actual pressure at the surface is not known from direct observation because of the refractive effects of the atmosphere on the stellar occultation data and those of the Pluto–Charon mutual events.

Tryka et al. (1994) determined the temperature of the N_2 surface of Pluto to be $T = 40 \pm 2$ K through a detailed study of the profile and strength of the 2.148 μm nitrogen absorption band in the planet's spectrum. This temperature is well within the β-N_2 phase boundary. At $T = 40$ K, the vapor pressure, P_v, of pure N_2 is 58 μbar; at $T = 38$ K, $P_v = 19$ μbar and at $T = 42$ K, $P_v = 159$ μbar (Brown and Ziegler 1979).

B. Direct Measurements

The detection of Pluto–Charon near their thermal emission peaks at 60 and 100 μm by the Infrared Astronomical Satellite (IRAS) demonstrated that the planet could not have an isothermal surface. The fluxes reported by various investigators studying the IRAS data are listed in Table II, from Tryka et al. (1994). Sykes et al. (1987) used models incorporating a latitudinal temperature distribution corresponding to that of a rapidly rotating body in radiative equilibrium with sunlight, and transferring surface ices (such as CH_4) by sublimation into colder, brighter isothermal polar caps, deriving an equatorial temperature of ~59 K. While 59 K appeared to agree with the result of Trafton and Stern (1983), the low emissivity adopted in their analysis would have made Pluto invisible to IRAS. Also, the high temperature coupled with conservation of energy required a latitudinal temperature gradient that could not be supported by a uniform distribution of methane ice over Pluto's surface. The more complex model computed by Sykes et al. (1987) is consistent with models of surface albedo distributions determined from Pluto's rotational lightcurve history by Marcialis (1983) and Buie (1984), but diverges from more recent millimeter-wave data by Stern et al. (1993) discussed below.

The thermal radiation from Pluto–Charon has been measured in the microwave spectral region; the fluxes reported by various investigators are given in Table II. Long wavelength measurements provide insight into Pluto's surface composition as well as its temperature, in part because the millimeter wavelength radiation arises from the subsurface at a depth depending upon the emissivity, transparency, and thermal structure of the first few centimeters below the "optical" (uppermost) surface. At wavelengths >800 μm there is less radiation from the Pluto–Charon pair than expected from an extrapolation of the fluxes from the IRAS observations, due to the presence of cold, N_2-sublimating regions (see the chapter by Spencer et al.).

In terms of albedo, Pluto has two basic surface units, with bright regions at high latitudes, and darker regions concentrated toward the equator (Buie et al. 1992; Young and Binzel 1993). The emitted flux received at the Earth is the sum of the thermal emission profiles of all these regions in view at the time of a given observation. Because bright surfaces absorb less sunlight, they should

TABLE II

Flux Measurements of Pluto and Charon

Wavelength (μm)	Flux (mJy)		Flux Corrected to IRAS Distance (mJy)		Source
25	40	±20			Aumann and Walker (1987)
60	420	±40	406	±38.7	Tedesco et al. (1987)
60	594	±14			Aumann and Walker (1987)
60	581	±58			Sykes et al. (1987)
100	727	±36.3			Aumann and Walker (1987)
100	721	±36			Sykes et al. (1987)
800	39	±6	35.1	±5.4	Jewitt (1994)
800	33	±7	32.2	±6.8	Stern et al. (1993)
1200	15.9	±4.5	14.8	±4.2	Altenhoff et al. (1988)
1200	10.7	±5.6	9.8	±5.1	Altenhoff et al. (1988)
1200	11.9	±4.6	10.8	±4.2	Altenhoff et al. (1988)
1200	15.5	±1.6	14.0	±1.4	Altenhoff et al. (1988)
1300	13	±4	11.7	±3.6	Jewitt (1994)
1300	12	±10	11.8	±9.8	Stern et al. (1993)
1300	10	±6	9.6	±5.8	Stern et al. (1993)
1300	15	±4.8	13.5	±4.3	Stern et al. (1993)

be colder than dark regions. However, this simple picture is complicated for surfaces covered by volatile ice, because the loss of latent heat through vaporization will reduce the temperature, or increase it if condensation occurs, tending to isothermalize the surface (Leighton and Murray 1966; Trafton and Stern 1983; Trafton 1984).

A warm (low albedo) region will radiate more energy at all wavelengths than a cold (higher albedo) region of equal area, and thus dominate the thermal emission. Similarly, the high-albedo area will dominate the visible/near-infrared (reflected light) portion of the spectrum. The radiation observed by IRAS arises primarily from the warm (probably) equatorial regions of the planet where solid N_2 is absent, while the bright, cold N_2 ice-covered regions contribute little to the thermal radiation of the planet (Sykes, unpublished manuscript). Thus, Pluto's surface can be modeled with two distinct temperature units corresponding to warm dark regions at equatorial latitudes (the IRAS detections), and higher-latitude cold bright frosts or ices, which give rise to the nitrogen atmosphere.

An analysis of all of the available radiometry of Pluto–Charon by Sykes (1993) indicates that the equatorial temperature of Pluto (together with Charon) in the mid-1980s was between 55 and 73 K. Sykes' models require some "infrared beaming," which is a phenomenon associated with local topography in which surface elements are heated by other elements within their field of view.

In principle, millimeter-wave observations detect the same thermal emis-

sion from the equatorial regions seen by IRAS, but at $\lambda \geq 800\,\mu$m the flux may be diminished by the lower temperature of the immediate subsurface and/or the lower emissivity of the surface materials at such wavelengths. If Pluto is considered a rapidly rotating body (insolation absorbed over the Sun-directed hemisphere and radiation occurring over the entire surface), the surface temperature at a given latitude is equal to the diurnal mean temperature (if the albedo is uniform at that latitude), and the diurnal skin depth is correspondingly small. Below the level of diurnal variation, the temperature trends toward the seasonal mean, which at Pluto's current epoch is very close to the diurnal mean temperature. Thus, the millimeter-wave fluxes, although they sample the temperature below the diurnal fluctuations, are still close to the surface temperature. Sykes et al. (1987), Stern et al. (1993), and Jewitt (1994) have calculated models in which lines of constant latitude are isotherms (equivalent to the rapid rotator model). However, the models of Tryka et al. (1994) show that Pluto can be considered a slow rotator with substantial temperature variation with time of day, latitude, and with depth in the immediate subsurface. They therefore reason that the millimeter-wave radiation arises from a depth of ~3 cm (this value depends upon the adopted value of the thermal inertia; Tryka et al. used $\sim 3 \times 10^4$ erg $s^{-1/2}cm^{-2}K^{-1}$), which is of the same order of magnitude of the expected penetration depth ($\sim 10\,\lambda$) of the long-wavelength radiation. As such, the mm-wave radiation arises in the region of mostly diurnal mean temperature, while the infrared radiation arises in the region undergoing diurnal variations.

Tryka et al. (1994) have synthesized all the direct thermal flux measurements given in Table II and the spectroscopically derived temperature (40 K) of the N_2-covered (polar) regions to calculate the extent of the N_2 polar caps and the temperature of the equatorial region. After the effect of Charon's thermal emission (which depends upon the assumed emissivity and measured albedo) is accounted for, a single composite gray-body flux curve can be drawn through all the thermal observations (Fig. 6), although the data at $\lambda > 800\,\mu$m fall systematically below the curve, possibly because the thermal emission at those wavelengths arises in the cooler subsurface, as noted above. An additional effect may be that the thermal emissivity of the surface is wavelength dependent (Stern et al. 1993), and has a value in the microwave region that is approximately half that at IRAS wavelengths (Sykes 1993, and an unpublished manuscript).

Improvements in the modeling of Pluto's temperature can be achieved with a better knowledge of the emissivities of the surface components; Stansberry et al. (1996) have made progress in an analysis of emissivities of various mixtures of Pluto's and Triton's surface constituents, focused particularly on the seasonal evolution of the surface–atmosphere interaction. Divergent points of view on the temperature structure of Pluto's surface and the contribution to the total thermal flux measurements of Pluto plus Charon remain to be resolved though improved data and modeling.

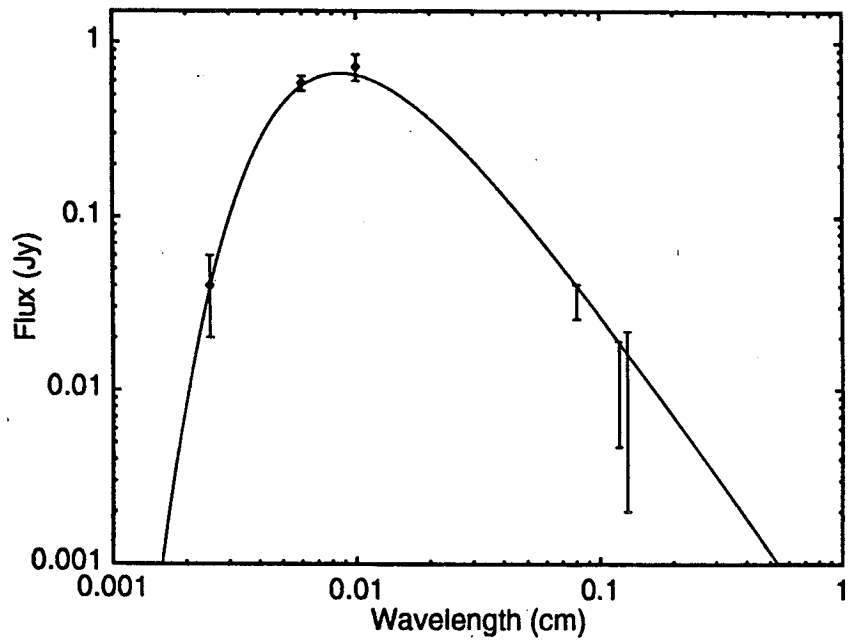

Figure 6. Observations (from Table II) and model of the thermal flux from the Pluto–Charon system. The infrared measurements are shown as points with standard errors. The millimeter wave points are represented by an error bar showing the range of measurements made at those wavelengths. The line is a model for the total flux from a system with an equatorial albedo of 0.2, polar caps of emissivity 0.6 extending to ±20 deg, and Charon albedo of 0.4 (figure from Tryka et al. 1995).

VI. GEOLOGY OF PLUTO

To speculate about the geology of Pluto and Charon within the limitations of the currently available data is risky. It is important to remember, for example, that we would anticipate that Ganymede and Callisto would have essentially identical geologies, given the same level of understanding that we presently have for the Pluto system. Triton is often cited as a possible Pluto analog. However, Triton's geologically recent, capture-induced, heating event has altered the surface of that satellite to an extent that we can expect great dissimilarities between it and Pluto. Our meager knowledge of the compositions of Pluto and Charon, in combination with a post-Voyager appreciation of other outer solar system icy objects, at least establishes criteria for identifying geologic questions we wish to address in upcoming investigations. Here we give a few examples.

A. Endogenic Processes

1. Tectonism. The Voyager survey of the outer solar system has revealed an astonishing variety of endogenic landforms on the surfaces of icy satellites

(see, e.g., Schenk and Moore 1995). Pluto and Charon's geologic history may have involved periods of internal expansion, perhaps due to a build-up of heat from tidal evolution, radiogenic sources or the freeze-expansion of a large internal H_2O layer. Such internal expansion would manifest itself on the surfaces of these objects in the form of normal faulting and graben formation. Normal faults are recognizable by their tendency to form traces that are rectilinear, arcuate, or else composed of sharply jointed or en-echelon straight segments. Graben are troughs formed by two inward-facing normal faults creating a down-dropped central block. Internal expansion of any spherical planetary object would result in global surface extension, causing the surface to split into scarp or graben-bounded polygons. The Uranian satellite Titania (diameter 1578 km) exhibits this form of global tectonism (Fig. 7).

Within the current uncertainty in the mass and radius of Pluto lies a bulk density that would imply that the H_2O ice in its mantle (if indeed the mantle is dominated by H_2O) would be undergoing conversion to ice II during the last half of solar system history (see the chapter by McKinnon et al.). The ongoing formation of an ice II inner mantle would cause the radius to shrink. This reduction in radius should, in turn, manifest itself in the form of large lateral compressional stresses in Pluto's crust. Geomorphic markers of this phenomena might be globally distributed thrust or reverse faults and tectonic ridges. Such features are characterized by their curvilinear-to-cuspate trace, and a transverse topographic profile frequently exhibiting upward convexity and strong slope asymmetry on either side of the crest. The observation of these landforms on Mercury (Fig. 8) was cited as evidence by Murray et al. (1974) for global lateral compression on that planet. Speculation that the theoretical critical value for the initiation of ice II formation lies within the present uncertainty in Pluto's bulk density, further emphasizes the utility of the detection/nondetection of compressional features as a test for Pluto (and, implicity, any other icy body) interior compositional and thermal models.

2. *Volcanics.* If Pluto or Charon exhibit evidence of volcanic activity, such observations can be used to constrain their compositions and thermal evolutions. Several planetary satellites imaged by the Voyager spacecraft show evidence of past or present volcanic activity. Given the rheology of ice (see reviews by Poirier [1982], and Consolmagno [1983]), it was not a surprise that "volcanism" on these objects usually has very little topographic expression. Even the best putative examples of volcanic landforms seen on Ariel, Miranda, Triton, and possibly Enceladus exhibit rarely more than a kilometer of relief (Jankowski and Squyres 1988; Pozio and Kargel 1989; Schenk 1991*a*; Croft et al. 1995; Shenk and Moore 1995). The most common evidence for volcanism on icy satellites is the presence of smooth, relatively craterless plains units on some of their surfaces (Fig. 7). These plains are thought to be emplaced as surface flows of liquid, liquid-ice slush or plastically deforming warm ice. A few examples of bright diffuse material mantling icy satellite terrain to either side of troughs have been interpreted as pyroclastic deposits (Smith et al. 1982).

Figure 7. Titania. The surface is broken by a network of scarps and graben, attesting to an expansion of its interior. Note the pit crater (diameter ~135 km), crossed by a graben, near the top limb. The region around the pit crater appears to be smooth and relatively craterless, perhaps the result of plains-forming volcanism specific to icy satellites (Voyager 2 image FDS 26843.15).

Even at the low temperatures of Pluto and Charon, the ices of nitrogen and methane are too weak to support more than ~100 m of topography (at scarps or flow fronts). Water ice and CO_2 ice can support greater relief but significantly higher temperatures are required to mobilize them. Faulting may form steep, high-standing topography in an H_2O-rich crust. The extent to which the H_2O recently detected in Pluto's spectrum reflects a sufficient amount to provide a strong crust has not yet been fully evaluated. Given the presence of low-temperature volatiles on Pluto, we cannot rule out the

Inverted

Figure 8. Compressional ridges on Mercury are evidence for a volumetric decrease of its interior. Note the two craters (the larger, lower one is ~55 km across) that have been cut and foreshortened by the thrust fault that forms the ridge. The presence of similar features on Pluto could be an indication of relatively recent and perhaps ongoing conversion of ice I into ice II in the planet's mantle (Mariner 10 mosaic).

Figure 9. Evolution of crater morphology with increasing diameter on icy targets. (left) ~20 km-diameter crater with central peak. (center) ~50 km-diameter crater with central pit. (right) ~80 km-diameter crater with topographic dome within its central pit. All examples are from Voyager 2 images of Ganymede (mosaic courtesy of P. M. Schenk).

possibility of eruptions of pyroclastic material that could form very large sheet-like deposits with very small slopes.

The plumes of Triton appear to represent a form of active outgasing (Smith et al. 1989; Kirk et al. 1995). Discovery of plumes or plume deposits on Pluto would serve to test the hypothesis of solar-powered Triton plumes because of the similarities in surface composition and (when Pluto is near perihelion) insolation.

B. Exogenic Processes

1. Cratering. If Pluto and Charon have not been heated by sources other than radiogenic, their surfaces may have preserved a record of the time-varying population of trans-Neptunian impactors. However, the predicted number of post-accretional craters may not be sufficient to saturate the surfaces of either Pluto or Charon over the age of the solar system (Weissman et al. 1989; Weissman and Stern 1994). This ultimately testable hypothesis implies that even very early resurfacing events may be recognizable from regional variations in crater density.

In addition to the importance of a wide range in crater distribution and sizes to crater statistics, is the information gained from crater morphology as a function of size and target. On icy satellites the transition diameter from one crater morphology to another scales to first order with gravity (Schenk 1991*b*). Pluto, with a surface gravity intermediate between large icy moons (e.g., Ganymede) and the middle-sized icy satellites (e.g., Titania) offers an opportunity to verify and constrain this apparent scaling further. For instance, craters with central pits are commonly observed on Ganymede and Callisto (Fig. 9) but rarely on middle-sized icy satellites (Fig. 7), perhaps as a consequence of the very large diameters such craters would have to achieve in the gravity regimes of middle-sized icy satellites (Schenk 1991*b*). If, in fact, central pit initiation is determined largely by gravity, then they should occur on Pluto in craters larger than ~60 to 70 km in diameter. Craters, and their ejecta deposits, also can serve as probes of crustal stratigraphy. Compositional investigations of materials excavated from depth by craters have been a useful tool for understanding the geology of the Moon (see, e.g., Hawke and Bell 1981) and Ganymede (Schenk and McKinnon 1985).

One or more concentric rings composed of ridges, scarps or graben surrounding very large impacts may form by the collapse of the transient crater when the excavation depth is comparable to the thickness of the lithosphere. This collapse can involve the prompt behavior of brittle material in the crater wall, as well as the much slower inward flow of plastically deforming asthenospheric material as the crater floor moves toward geoid equilibrium. All of these factors affect the number, spacing and morphology of the rings (McKinnon and Melosh 1980). In extreme cases, these rings might girdle a planetary object; one example is Ithaca Chasma, a trough system of global scale extending at least 270 deg around Tethys and "centered" around the gigantic Odysseus impact feature (Smith et al. 1982; Moore and Ahern 1983). Multi-

3

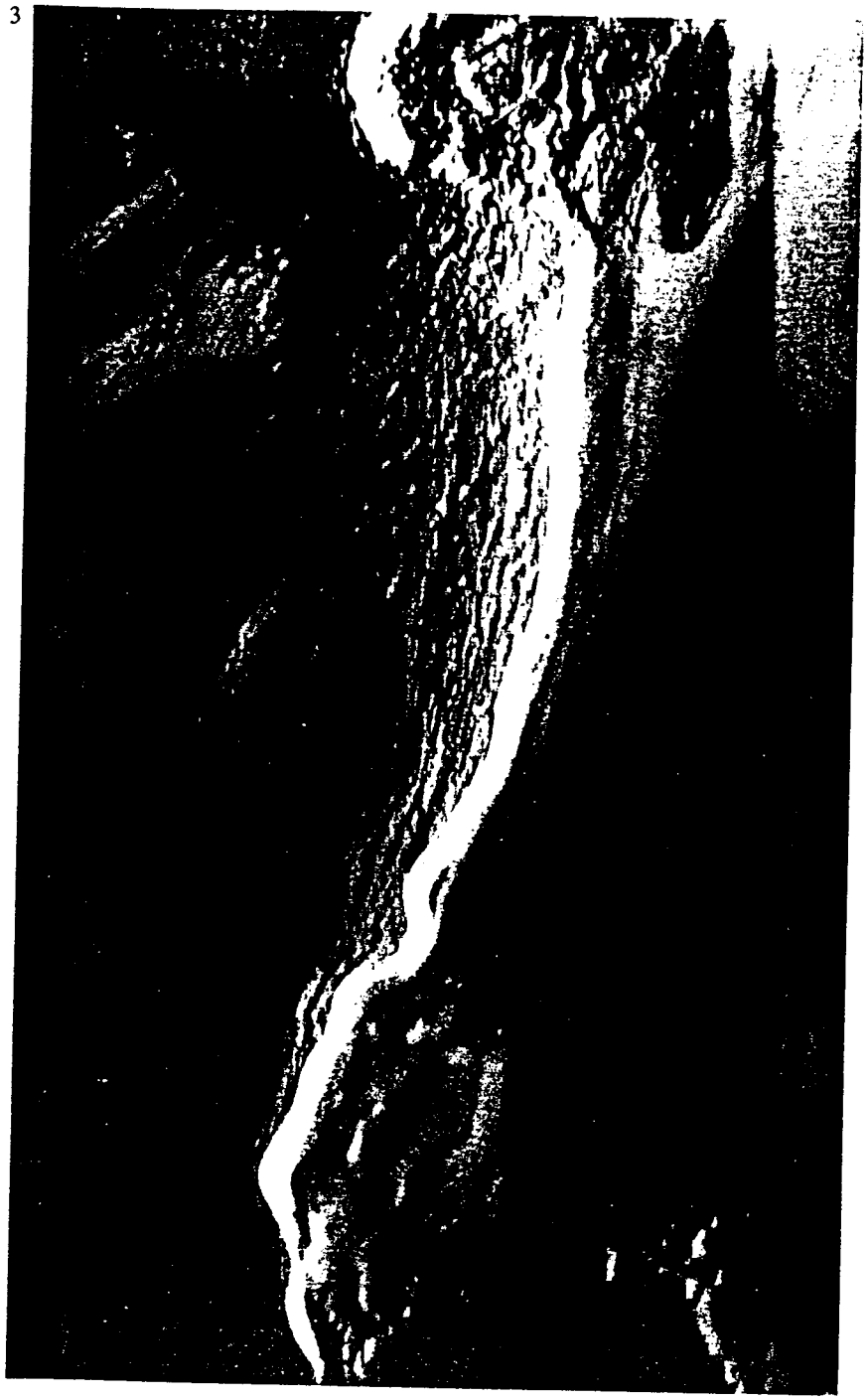

Figure 10. Erosion in the south polar region of Mars in which sublimation of a volatile incorporated into the original deposit has played a major role. Retreating scarps; the retreat is demonstrated by the absence of secondary craters on the lower surface beyond the scarp wall to the right of the image, but which are still visible on the upper surface, from the breached 25 km-diameter crater at the top edge of the figure. The image is ~150 km from top to bottom (Viking Orbiter image 421B79).

ring basins, if present on Pluto or Charon, offer the possibility to estimate lithospheric thickness and other properties at the time of basin formation.

On the Moon and Mercury, regions located antipodal to very large impact features are covered with rugged, equidimensional hills or mounds, and narrow linear troughs or grooves. These landforms have been attributed to the degradation of pre-existing topography by focused seismic energy from the basin-forming impacts. There is some evidence for similarly formed features on the middle-sized icy satellites Tethys and Rhea (Watts et al. 1991; Moore et al. 1996*a*). In extreme cases, a seismically shaken surface would be reduced to a level plain. The ability of a planetary body to focus seismic energy toward the antipode of an impact is thought to be governed by the size and density contrasts of internal layers (see, e.g., Hughes et al. 1977; Watts et al. 1991; Moore et al. 1996*a*). The amount and extent of antipodal damage may be a crude tomographic measure, although ice-rich planetary interiors, such as Pluto and Triton, may have responded differently from completely rocky planets. Regions on Triton and Pluto that are antipodal to very large impacts should be examined for pre-existing landforms which have been degraded in this manner.

2. *Sublimation-Driven Degradation.* The polar terrains of Mars are covered in many places with irregular pits and retreating scarps (Sharp 1973). These features are diagnostic of exogenic degradation due to the loss of a volatile rock-forming matrix or cement (see Figs. 10 and 11). It has been generally unrecognized that the same (or very similar) geologic process responsible for the Martian polar terrains also operates on some of the outer-planet satellites (Moore et al. 1993,1996*b*). For instance, the development of many of the scarps on Triton, and the depressions they surround, appears to involve a process called scarp recession, as the planimetric traces of these structures are inconsistent with formation either by faulting or as flow fronts (Moore and Spencer 1990). Scarp recession can occur on the Earth when a structural or stratigraphic inhomogeneity near the scarp base is mechanically weakened. Because conditions on Triton are unfavorable for some of the processes which cause scarp recession, such as erosion by abrasion from wind or channelized running fluid, mechanical weakening of material exposed in the face of a scarp probably involves the loss of a cementing or matrix-forming material by sublimation. A somewhat similar hypothesis has been offered for the formation of scarps and enclosed depressions on Io (McCauley et al. 1979). The proposed seasonally driven fluctuation in the mass of Pluto's atmosphere (see, e.g., Cruikshank and Silvaggio 1980; Stern et al. 1988) in combination with the widespread occurrence of the highly volatile N_2 (Owen et al. 1993*a*), implies that landforms modified by repeated episodes of sublimation and erosion might be seen.

3. *Aeolian Activity.* Current estimates constrain the surface pressure of Pluto's N_2-dominated atmosphere broadly between ~160 and 3 μbar (see Sec. V.1; chapters by Yelle and Elliot, and by Spencer et al.; Stansberry et al. 1994), which is comparable with Triton (P_s~14 μbar) (see, e.g., Broadfoot

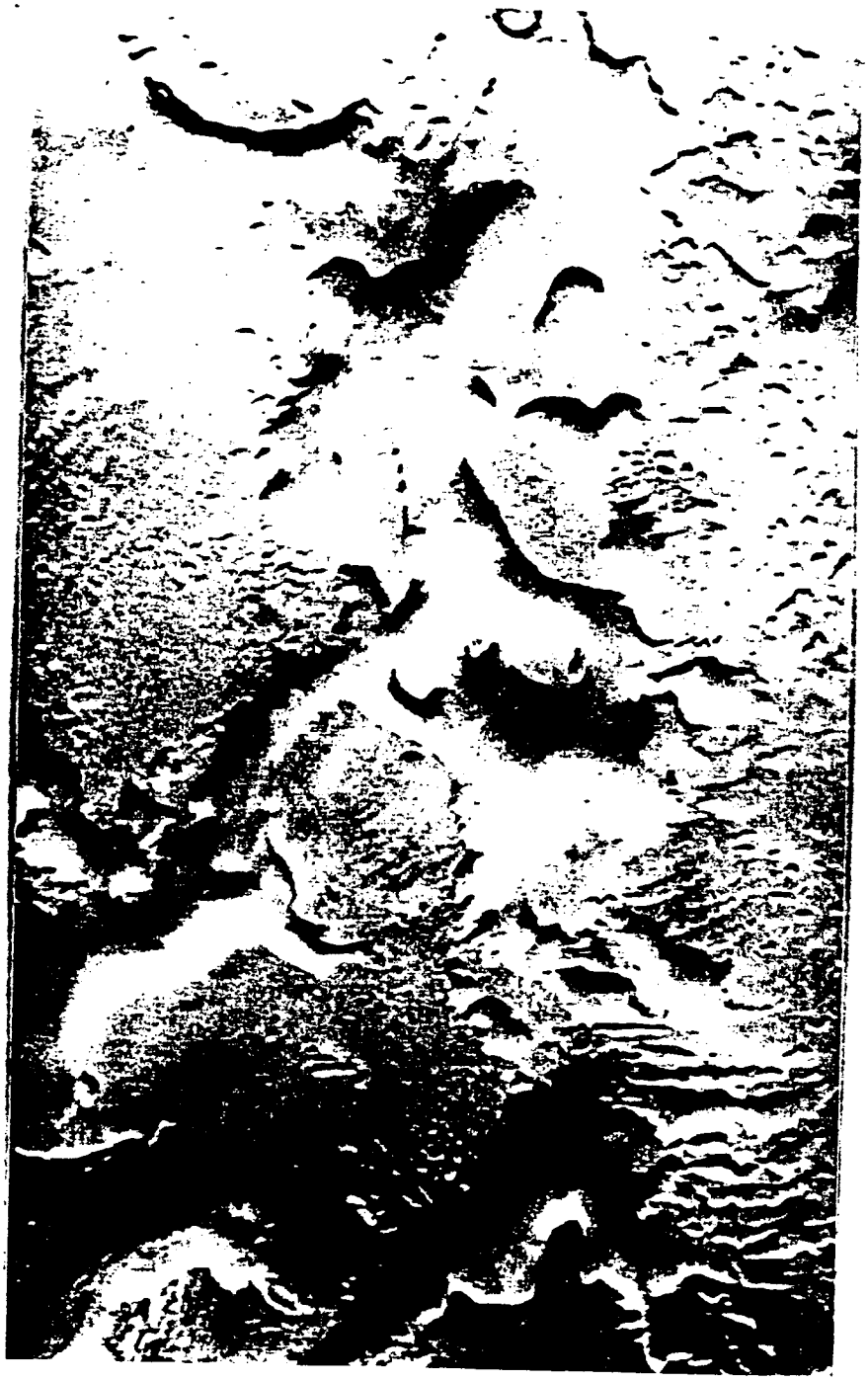

Figure 11. Etched and pitted terrain on Mars; a formerly horizontal surface has been substantially eroded, probably through the combined effects of strata disaggregation due to the loss of a volatile matrix or cement, followed by the removal of detrital refractory fines by the wind. The image is ~190 km from top to bottom (Viking Orbiter image 390B90).

et al. 1989; Tyler et al. 1989). The possibility of aeolian activity on Pluto arises from the surprising discovery of dark deposits of apparently wind-blown particulates on Triton (see, e.g., Smith et al. 1989) (Fig. 12). Following the formulation of Chyba and Sagan (1990), and assuming that the atmospheric dynamics are similar to those of Triton (Ingersoll 1990), we note that the wind speed on Pluto may be as much as an order of magnitute too low to initiate saltation of sand sized particles if $P_s < 50\ \mu$bar. For the case of $P_s \geq 50\ \mu$bar, the saltation threshold wind speed on Pluto is in the range of maximum surface wind speeds theoretically achievable on the planet, and the detection of landforms created by saltating particles (e.g., sand dunes; Fig. 13) may provide an indicator of periods of high atmospheric pressures on the planet.

The winds of Pluto may still play a role in particle distribution even if the surface pressures are as low as $\sim 10\ \mu$bar. Material thrown into the atmosphere by endogenic processes or by impact events will settle to the surface along a path defined by the wind direction. Chyba and Sagan (1990), following the explanation proposed for wind-driven changes at high Martian altitudes (see, e.g., Sagan et al. 1974), suggest that μm-scale surface material on Triton's surface may be picked up and moved by the wind if the interparticle cohesion is very low or nonexistent. Dust devil-like vortices, if they exist in Pluto's boundary layer, would greatly increase the likelihood that these particles of little or no cohesion (including those with sizes up to the $100\ \mu$m-range) could be lofted, even if the atmosphere is as "thin" as Triton's (Ingersoll and Tryka 1990). Of course, low-cohesion particles are unlikely to form deposits with topographic expression (such as sand dunes) but would instead create surface-coating streaks.

The information returned during the first thirty years of robotic planetary exploration has given us insight into the surface structures of not only rocky bodies, but at least 25 icy bodies, thus providing a basis for speculation about the geology of Pluto and its satellite. In particular, the opportunity to observe Triton closely from Voyager 2 was especially useful because of the similar sizes, densities, and surface compositions of Pluto and Triton. Looking toward an opportunity to send spacecraft to the Pluto–Charon system has encouraged this speculation regarding geologic processes and the implications of their presence or absence on these bodies. However, in the spirit of the experiences with each planet, satellite, or asteroid newly visited, we should anticipate discovering wholly unexpected features on the surfaces of Pluto and Charon in any initial *in situ* spacecraft investigation.

VII. PLUTO AMONG THE ICY BODIES OF THE OUTER SOLAR SYSTEM

For 46 years after the discovery of Pluto, little information existed on the dimensions, mass, and composition of the most distant planet (Hoyt 1980). When frozen methane was detected in 1976 (Cruikshank et al. 1976), a high surface albedo was indicated, suggesting that if Pluto has a bulk density that

Figure 12. Landforms created from aeolian deposits. Streaks of dark material on Triton, tranported by the wind. This very fine material, which is either emplaced directly as plume fallout or else saltated from an upwind ground source (or both), resembles wind streaks on Mars, and attests to the ability of even very low density atmospheres to generate aeolian features. The scene covers ~650 km from top to bottom (Voyager 2).

includes a volatile fraction, both the diameter and the mass are substantially smaller than previously estimated on the basis of the putative perturbations on the orbits of Neptune and Uranus. This assertion was substantiated with the discovery of Charon in 1978 (Christy and Harrington 1978), allowing the first observationally based computation of the planet's mass (Harrington and Christy 1980).

Remarkably, in less than two decades our knowledge and understanding of the Pluto–Charon system has expanded to the point that a book of this size has been written, and detailed plans for a space mission are in an advanced state of development.

As we described in this chapter, Pluto shares many properties with Triton; size, density, temperature, surface composition, and a tenuous atmosphere, yet the differences between the two bodies are significant, even if largely still unknown. These two bodies share the defining property of surface ices dominated by frozen nitrogen. Whether or not frozen nitrogen is a significant component of icy planetesimals in the Kuiper belt or the Oort cloud is not yet known. In any event, the appearance of N_2 at the edge of the planetary system marks a clear departure from the H_2O-ice rich surfaces of the other icy bodies of the outer solar system (e.g., the satellites of Jupiter, Saturn, and Uranus), including Charon itself. As discussed in the chapter by McKinnon et al., the interior of Pluto must contain H_2O ice, even though its surface is largely covered by the much more volatile N_2.

Those bodies with H_2O-ice dominated surfaces exhibit a wide range of morphologies and photometric properties. The icy satellite surfaces differ from one another in age, amount of space weathering, and degree of contamination by (largely) unknown materials. Consequently, it appears that no two are the same when considered in detail. Certainly there is no single model for the origin and development of an icy satellite surface, although at least 16 satellites have surfaces dominated spectrally by H_2O-ice. It is therefore perhaps naive to expect Triton and Pluto to exhibit similar surface morphologies at the level of geologic structures or surface microstructure.

Triton and Pluto probably result from the formation of planetary embryos in the solar nebula some 30 to 40 AU from the new Sun. Their inventories of volatiles and organic materials are a window on the chemical composition, processes and histories in this region of the solar nebula. While the presence of highly volatile surface ices may have resulted from emplacement from exogenous sources and therefore have little bearing on the materials from which they originated, N_2 may have been an important initial constituent of these two bodies, and internal heating events drove it to the surface sometime after planet formation.

In any event, from the point of view of their surface and bulk volatile contents, Pluto and Triton are likely to emerge as keystone objects as we continue the exploration of the Kuiper disk of planetesimals that appears to extend the icy fringes of the solar system well beyond the boundary defined by the major planets (Jewitt and Luu 1995; chapter by Weissman and Levison).

Figure 13. Landforms created from aeolian deposits. Sand dunes on Mars. Dark barchan dunes crossing a surface covered by seasonal CO_2 frost. The streamers from the horns of the dunes may be evidence of active saltation, which is transporting sand across the top of the frost. Image ~40 km from top to bottom (Viking Orbiter image 544B05).

Acknowledgments. This research is supported by a NASA grant through the Planetary Astronomy and Planetary Geology and Geophysics Programs. We thank R. N. Clark, R. L. Kirk, R. M. Nelson, B. Schmitt, J. A. Stansberry, S. A. Stern, D. J. Tholen, and L. A. Young for very helpful reviews of the original manuscript.

REFERENCES

Allamandola, L. J. 1984. Absorption and emission characteristics of interstellar dust. In *Galactic and Extragalactic Infrared Spectroscopy*, eds. M. F. Kessler and J. P. Phillips (Dordrecht: D. Reidel), pp. 5–35.

Altenhoff, W. J., Chini, R., Hein, H., Kreysa, E., Mezger, P. G., Salter, C., and Schraml, J. B. 1988. First radio astronomical estimate of the temperature of Pluto. *Astron. Astrophys.* 190:L15–L17.

Apt, J., Carleton, N. P., and MacKay, C. D. 1983. Methane on Triton and Pluto: New CCD spectra. *Astrophys. J.* 270:342–350.

Aumann, H. H., and Walker, R. G. 1987. IRAS observations of the Pluto–Charon system. *Astron. J.* 94:1088–1091.

Barker, E. S., Cochran, W. D., and Cochran, A. L. 1980. Spectrophotometry of Pluto from 3500 to 7350 Å. *Icarus* 44:43–52.

Bell, J. F., Clark, R. N., McCord, T. B., and Cruikshank, D. P. 1979. Reflection spectra of Pluto and three distant satellites. *Bull. Amer. Astron. Soc.* 11:570 (abstract).

Binzel, R. P. 1988. Hemispherical color differences on Pluto and Charon. *Science* 241:1070–1072.

Bohn, R. B., Sandford, S. A., Allamandola, L. J., and Cruikshank, D. P. 1994. Infrared spectroscopy of Triton and Pluto ice analogs: The case for saturated hydrocarbons. *Icarus* 111:151–173.

Bosh, A. S., Young, L. A., Elliot, J. L., Hammel, H. B., and Baron, R. L. 1992. Photometric variability of Charon at 2.2 μm. *Icarus* 95:319–324.

Broadfoot, A. L., Atreya, S. K., Bertaux, J. L., Blamont, J. E., Dessler, A. J., Donahue, T. M., Forrester, W. T., Hall, D. T., Herbert, F., Holberg, J. B., Hunten, D. M., Krasnopolsky, V. A., Linick, S., Lunine, J. I., McConnell, J. C., Moos, H. W., Sandel, B. R., Schneider, N. M., Shemansky, D. E., Smith, G. R., Strobel, D. F., and Yelle, R. V. 1989. Ultraviolet spectrometer observations of Neptune and Triton. *Science* 246:1459–1465.

Brown, G. N., Jr., and Ziegler, W. T. 1979. Vapor pressure and heats of vaporization and sublimation of liquids and solids of interest in cryogenics below 1-atm pressure. In *Advances in Cryogenic Engineering*, vol. 25, eds. K. D. Timmerhaus and H. A. Snyder (New York: Plenum Press), pp. 662–670.

Brown, R. H., Cruikshank, D. P., Veverka, J., Helfenstein, P., and Eluszciewicz, J. 1995. Surface composition and photometric properties of Triton. In *Neptune and Triton*, ed. D. P. Cruikshank (Tucson: Univ. Arizona Press), pp. 991–1030.

Buie, M. W. 1984. Lightcurve CCD Spectrophotometry of Pluto. Ph.D. Thesis, Univ. of Arizona.

Buie, M. W., Cruikshank, D. P., Lebofsky, L. A., and Tedesco, E. F. 1987. Water frost on Charon. *Nature* 329:522–523.

Buie, M. W., and Fink, U. 1984. Methane frost on Pluto: Model implications from spectrophotometry. *Bull. Amer. Astron. Soc.* 16:651 (abstract).

Buie, M. W., and Fink, U. 1987. Methane absorption variations in the spectrum of Pluto. *Icarus* 70:483–498.

Buie, M. W., and Shriver, S. K. 1994. The distribution of water frost on Charon. *Icarus* 108:225–233.

Buie, M. W., Tholen, D. J., and Horn, K. 1992. Albedo maps of Pluto and Charon: Initial mutual event results. *Icarus* 97:211–227.

Buie, M. W., Wasserman, L. H., and Tholen, D. J. 1994. The separate lightcurves of Pluto and Charon from Hubble Space Telescope imaging. *Bull. Amer. Astron. Soc.* 26:1169 (abstract).

Calvin, W. M., Clark, R. N., Brown, R. H., and Spencer, J. R. 1995. Spectra of the icy Galilean satellites from 0.2 to 5 μm: A compilation, new observations, and a recent summary. *J. Geophys. Res.* 100:19041–19048.

Chandrasekhar, S. 1960. *Radiative Transfer* (New York: Dover).

Christy, J. W., and Harrington, R. S. 1978. The satellite of Pluto. *Astron. J.* 83:1005–1008.

Chyba, C., and Sagan C. 1990. Triton's streaks as windblown dust. *Nature* 346:546–548.

Clark, R. N., Fanale, F. P., and Zent, A. P. 1983. Frost grain size metamorphism: Implications for remote sensing of planetary surfaces. *Icarus* 56:233–245.

Clark, R. N., Fanale, F. P., and Gaffey, M. J. 1986. Surface composition of natural satellites. In *Satellites*, eds. J. A. Burns and M. S. Matthews (Tucson: Univ. Arizona Press), pp. 437–491.

Consolmagno, G. J. 1983. Ice-rich planets and the physical properties of ice. *J. Phys. Chem.* 87:4204–4208.

Croft, S. K., Kargel, J. S., Kirk, R. L., Moore, J. M., Schenk, P. M., and Strom, R. G. 1995. The geology of Triton. In *Neptune and Triton*, ed. D. P. Cruikshank (Tucson: Univ. Arizona Press), pp. 879–947.

Cruikshank, D. P., and Brown, R. H. 1986. Satellites of Uranus and Neptune, and the Pluto–Charon system. In *Satellites*, eds. J. A. Burns and M. S. Matthews (Tucson: Univ. Arizona Press), pp. 836–873.

Cruikshank, D. P., and Silvaggio, P. M. 1980. The surface and atmosphere of Pluto. *Icarus* 41:96–102.

Cruikshank, D. P., Pilcher, C. B., and Morrison, D. 1976. Pluto: Evidence for methane frost. *Science* 194:835–837.

Cruikshank, D. P., Roush, T. L., Owen, T. C., Geballe, T. R., de Bergh, C., Schmitt, B., Brown, R. H., and Bartholomew, M. J. 1993. Ices on the Surface of Triton. *Science* 261:742–745.

Domingue, D. L., Hapke, B. W., Lockwood, G. W., and Thompson, D. T. 1991. Europa's phase curve: Implications for surface structure. *Icarus* 90:30–42.

Duxbury, N. S., and Brown, R. H. 1993. The phase composition of Triton's polar caps. *Science* 261:748–751.

Elliot, J. L., Dunham, E. W., Bosh, A. S., Slivan, S. M., Young, L. A., Wasserman, L. H., and Millis, R. L. 1989. Pluto's atmosphere. *Icarus* 77:148–170.

Eluszkiewicz, J. 1991. On the microphysical state of the surface of Triton. *J. Geophys. Res.* 96:19217–19229.

Fink, U., Smith, B., Benner, D., Johnson, J., Reitsema, H., and Westphal J. 1980. Detection of a CH_4 atmosphere on Pluto. *Icarus* 44:62–71.

Fink, U., and DiSanti, M. A. 1988. The separate spectra of Pluto and its satellite Charon. *Astron. J.* 95:229–236.

Green, J. R., Brown, R. H., Cruikshank, D. P., and Anicich V. 1991. The absorption coefficient of nitrogen with application to Triton. *Bull. Amer. Astron. Soc.*

23:1208 (abstract).
Grundy, W. M. 1995. Methane and Nitrogen Ices on Pluto and Triton: A Combined Laboratory and Telescope Investigation. Ph.D. Thesis, Univ. Arizona.
Grundy, W. M., and Fink, U. 1993. CCD spectra of Pluto from 1982 to present. *Bull. Amer. Astron. Soc.* 25:1131 (abstract).
Grundy, W. M., Schmitt, B., and Quirico, E. 1993. The temperature-dependent spectra of α and β nitrogen ice with application to Triton. *Icarus* 105:254–258.
Grundy, W. M., Quirico, E., and Schmitt, B. 1996. The temperature dependent spectrum of methane ice between 14000 and 3000 cm^{-1} with application to Triton and Pluto. In preparation.
Hapke, B. W. 1981. Bidirectional reflectance spectroscopy I. Theory. *J. Geophys. Res.* 86:3039–3054.
Hapke, B. W. 1984. Bidirectional reflectance spectroscopy 3. Correction for macroscopic roughness. *Icarus* 59:41–59.
Hapke, B. W. 1986. Bidirectional reflectance spectroscopy 4. The extinction coefficient and the opposition effect. *Icarus* 67:264–280.
Hapke, B. W. 1993*a*. Combined theory of reflectance and emittance spectroscopy. In *Remote Geochemical Analysis: Elemental and Mineralogical Composition*, eds. C. M. Pieters and P. A. J. Englert (New York: Cambridge Univ. Press), pp. 31–42.
Hapke, B. W. 1993*b*. *Reflectance and Emittance Spectroscopy* (New York: Cambridge Univ. Press).
Hardie, R. H. 1965. A re-examination of the light variation of Pluto. *Astron. J.* 70:140 (abstract).
Harrington, R. S., and Christy, J. W. 1980. The satellite of Pluto. II. *Astron. J.* 85:168–170.
Hawke, B. R., and Bell, J. F. 1981. Remote sensing studies of lunar dark-halo impact craters: Preliminary results and implications for early volcanism. *Proc. Lunar Planet. Sci. Conf.* 12B:665–678.
Helfenstein, P., Veverka, J., and Thomas, P. C. 1988. Uranus Satellites: Hapke parameters from Voyager disk-integrated photometry. *Icarus* 74:321–239.
Hoyt, W. G. 1980. *Planets X and Pluto* (Tucson: Univ. of Arizona Press).
Hudgins, D. M., Sandford, S. A., Allamandola, L. J., and Tielens, A. G. G. M. 1993. Mid- and far-infrared spectroscopy of ices: Optical constants and integrated absorbances. *Astrophys. J. Suppl.* 86:713–870.
Hubbard, W. B., Hunten, D. M., Dieters, S. W., Hill, K. M., and Watson, R. D. 1988. Occultation evidence for an atmosphere on Pluto. *Nature* 336:452–454.
Hughes, H. G., App, F. N., and McGetchen, T. R. 1977. Global seismic effects of basin-forming impacts. *Phys. Earth Planet. Int.* 15:251–263.
Ingersoll, A. P. 1990. Dynamics of Triton's atmosphere. *Nature* 344:315–317.
Ingersoll, A. P., and Tryka, K. A. 1990. Triton's plumes: The dust devil hypothesis. *Science* 250:435–437.
Jankowski, D. G., and Squyres, S. W. 1988. Solid-state ice volcanism on the satellites of Uranus. *Science* 241:1322–1325.
Jewitt, D. C. 1994. Heat from Pluto. *Astron. J.* 107:372–378.
Jewitt, D. C., and Luu, J. 1995. The solar system beyond Neptune. *Astron. J.* 109:1867–1876.
Khare, B. N., Thompson, W. R., Sagan, C., Arakawa, E. T., Brueil, C., Judish, J. P., Khanna, R. K., and Pollack, J. B. 1990. Optical constants of solid methane. In *First Intl. Conf. on Laboratory Research for Planetary Atmospheres*, eds. K. Fox, J. E. Allen, Jr. and D. T. Quillen, NASA CP-3077, pp. 327–339.
Kirk, R. L., Soderblom, L. A., Brown, R. H., Kieffer, S. W., and Kargel, J. S. 1995. Triton's plumes: Discovery, characteristics, and models. In *Neptune and Triton*, ed. D. P. Cruikshank (Tucson: Univ. Arizona Press), pp. 949–989.

Leighton, R. B., and Murray, B. C. 1966. Behavior of carbon dioxide and other volatiles on Mars. *Science* 153:136–144.

Löwen, H. W., Bier, K. D., and Jodl, H. J. 1990. Vibron-phonon excitations in the molecular crystals N_2, O_2, and CO by Fourier transform infrared and Raman studies. *J. Chem. Phys.* 93:8565–8575.

Marcialis, R. L. 1983. A Two-Spot Model for the Surface of Pluto. Master's Thesis, Vanderbilt University.

Marcialis, R. L., and Lebofsky, L. A. 1991. CVF spectrophotometry of Pluto. *Icarus* 89:255–263.

Marcialis, R. L., Rieke, G. H., and Lebofsky, L. A. 1987. The surface composition of Charon: Tentative identification of water ice. *Science* 237:1349–1351.

Marcialis, R. L., Lebofsky, L. A., DiSanti, M. A., Fink, U., Tedesco, E. F., and Africano, J. 1992. The albedos of Pluto and Charon: Wavelength dependence. *Astron. J.* 103:1389–1394.

McCauley, J. F., Smith, B. A., and Soderblom, L. A. 1979. Erosional scarps on Io. *Nature* 280:736–738.

McKinnon, W. B., and Melosh, H. J. 1980. Evolution of planetary lithospheres: Evidence from multiringed structures on Ganymede and Callisto. *Icarus* 44:454–471.

Millis, R. L., Wasserman, L. H., Franz, O. G., Nye, R. A., Gilmore, A. C., Kilmartin, P. M., Allen, W. H., Watson, R. D., Dieters, S. W., Hill, K. M., Giles, A. B., Blow, G., Priestley, J., Walker, W. S. G., Marino, B. F., Dix, D. G., Page, A., Kennedy, H. D., Elliot, J. L., Dunham, E., Bosh, A. S., Young, L. A., Slivan, S. M., and Klemola, A. R. 1988. Observations of the 9 June 1988 occultation by Pluto. *Bull. Amer. Astron. Soc.* 20:806 (abstract).

Moore, J. M., and Ahern, J. L. 1983. The geology of Tethys. *J. Geophys. Res.* 88:577–584.

Moore, J. M., and Spencer, J. R. 1990. Koyaanismuuyaw: The hypothesis of a perennially dichotomous Triton. *Geophys. Res. Lett.* 17:1757–1760.

Moore, J. M., Zent, A. P., and Cruikshank, D. P. 1993. Mass wasting and ground collapse in terrains of volatile-rich deposits on Mars and some outer-planet satellites. *Bull. Amer. Astron. Soc.* 25:1112 (abstract).

Moore, J. M, Asphaug, E., and McKinnon, W. B. 1996*a*. Large impact features on middle-sized icy satellites: Numerical modeling of prompt effects and analytical modeling of delayed effects. *Icarus*, submitted.

Moore, J. M., Mellon, M. T., and Zent, A. P. 1996*b*. Mass wasting and ground collapse in terrains of volatile-rich deposits as a solar system-wide geological process: The pre-Galileo view. *Icarus*, in press.

Murray, B. C., Belton, M. J. S., Danielson, G. E., Davies, M. E., Gault, D. E., Hapke, B., O'Leary, B., Strom, R. G., Suomi, V., and Trask, N. 1974. Mercury's surface: Preliminary description and interpretation from Mariner 10 pictures. *Science* 185:169–179.

Olkin, C. B., Young, L. A., Elliot, J. L., Tholen, D. T., and Buie, M. W. 1993. Individual light curves of Pluto and Charon. *Bull. Amer. Astron. Soc.* 25:1132–1133 (abstract).

Owen, T. C., Roush, T. L., Cruikshank, D. P., Elliot, J. L., Young, L. A., de Bergh, C., Schmitt, B., Geballe, T. R., Brown, R. H. and Bartholomew, M. J. 1993*a*. Surface ices and atmospheric composition of Pluto. *Science* 261:745–748.

Owen, T. C., Cruikshank, D. P., de Bergh, C., Geballe, T. R., Roush, T., Bartholomew, M. J., Schmitt, B., Brown, R. H., Elliot, J. L., Young, L. A., and Douté, S. 1993*b*. New spectra of Pluto in the 1.2–2.5 μm range. *Bull. Amer. Astron. Soc.* 25:1128 (abstract).

Owen, T. C., Cruikshank, D. P., Roush, T., Geballe, T. R., and de Bergh, C. 1996.

Water ice on Pluto. In preparation.
Poirier, J. P. 1982. Rheology of ices: A key to the tectonics of the ice moons of Jupiter and Saturn. *Nature* 299:683–688.
Pozio, S., and Kargel, J. S. 1989. The tectonic and igneous evolution of Enceladus. *Lunar Planet. Sci. Conf.* XX:864–865 (abstract).
Quirico, E., and Schmitt, B. 1996. Near infrared spectroscopy of simple hydrocarbons and carbon ices diluted in solid N_2 and as pure ices: Implications for Triton and Pluto. In preparation.
Roush, T. L. 1994. Charon: More than water ice? *Icarus* 108:243–254.
Roush, T. L. 1996. Near-IR (0.8–2.5 μm) optical constants of water ice at 100 K. *Lunar Planet. Sci. Conf.* XXVII, submitted.
Roush, T. L., Pollack, J. B., Witteborn, F. C., Bregman, J., and Simpson, J. P. 1990. Ice and minerals on Callisto: A reassessment of the reflectance spectra. *Icarus* 86:355–382.
Roush, T. L., Cruikshank, D. P., Pollack, J. B., Young, E. F., and Bartholomew, M. J. 1996. Near-infrared spectral geometric albedos of Charon and Pluto: Constraints on Charon's surface composition. *Icarus* 119:214–218.
Roush, T. L., Cruikshank, D. P., and Owen, T. C. 1995. Surface ices in the outer solar system. In *Volatiles in the Earth and Solar System*, ed. K. A. Farley (??:??), pp. 143–153.
Sagan, C., Veverka, J., Steinbacher, R., Quam, L., Tucker, R., and Eross, B. 1974. Variable features on Mars IV. Pavonis Mons. *Icarus* 22:24–47.
Sawyer, S. R. 1989. Reflectance spectroscopy of the surface and atmosphere of Pluto–Charon. *Bull. Amer. Astron. Soc.* 21:986 (abstract).
Schenk, P. M. 1991*a*. Fluid volcanism on Miranda and Ariel: Flow morphology and composition. *J. Geophys. Res.* 96:1887–1906.
Schenk, P. M. 1991*b*. Ganymede and Callisto: Complex crater formation and planetary crusts. *J. Geophys. Res.* 96:15635–15664.
Schenk, P. M., and McKinnon, W. B. 1985. Dark halo craters and the thickness of grooved terrain on Ganymede. *J. Geophys. Res.* 90:775–783.
Schenk, P. M., and Moore, J. M. 1995. Volcanic constructs on Ganymede and Enceladus: Topographic evidence from stereo images and photoclinometry. *J. Geophys. Res.* 100:19009–19022.
Schmitt, B., and Quirico, E. 1992. Laboratory data on near-infrared spectra of ices of planetary interest. *Bull. Amer. Astron. Soc.* 24:968 (abstract).
Schmitt, B., Quirico, E., and Lellouch, E. 1992. Near infrared spectra of potential solids at the surface of Titan. In *Proceedings of a Symposium on Titan*, ESA SP-338 (Noordwijk: European Space Agency), pp. 383–388.
Schmitt, B., Quirico, E., de Bergh, C., Owen, T. C., and Cruikshank, D. P. 1993. The near-infrared spectra of Triton and Pluto: A laboratory analysis of the methane bands. *Bull. Amer. Astron. Soc.* 25:1129 (abstract).
Schmitt, B., Douté, S., Quirico, E., Benchkoura, A., de Bergh, C., Owen, T. C., and Cruikshank, D. P. 1994. The state and composition of the surface of Pluto: Laboratory experiments and numerical modeling. *Bull. Amer. Astron. Soc.* 26:1170 (abstract).
Scott, T. A. 1976. Solid and liquid nitrogen. *Phys. Repts.* 27:89–157.
Sharp, R. G. 1973. Mars: South polar pits and etched terrain. *J. Geophys. Res.* 78:4222–4230.
Smith, B. A., Soderblom, L. A., Batson, R., Bridges, P., Inge, J., Masursky, H., Shoemaker, E. M., Beebe, R. F., Boyce, J. M., Briggs, G. A., Bunker, A., Collins, S. A., Hansen, C. J., Johnson, T. V., Mitchell, J. L., Terrile, R. J., Cook, A. F., Cuzzi, J. N., Pollack, J. B., Danielson, G. E., Ingersoll, A. P., Davies, M. E., Hunt, G. E., Morrison, D., Owen, T., Sagan, C., Veverka, J., Strom, R., and Suomi,

V. E. 1982. A new look at the Saturn system: The Voyager 2 images. *Science* 215:504–537.

Smith, B. A., Soderblom, L. A., Banfield, D., Barnet, C., Basilevsky, A. T., Beebe, R. F., Bollinger, K., Boyce, J. M., Brahic, A., Briggs, G. A., Brown, R. H., Chyba, C., Collins, S. A., Colvin, T., Cook, A. F., II, Crisp, D., Croft, S. K., Cruikshank, D., Cuzzi, J. N., Danielson, G. E., Davies, M. E., De Jong, E., Dones, L., Godfrey, D., Goguen, J., Grenier, I., Haemmerle, V. R., Hammel, H., Hansen, C. J., Helfenstein, C. P., Howell, C., Hunt, G. E., Ingersoll, A. P., Johnson, T. V., Kargel, J., Kirk, R., Kuehn, D. I., Limaye, S., Masursky, H., McEwen, A., Morrison, D., Owen, T., Owen, W., Pollack, J. B., Porco, C. C., Rages, K., Showalter, M., Sicardy, B., Simonelli, D., Spencer, J., Sromovsky, B., Stoker, C., Strom, R. G., Suomi, V. E., Synott, S. P., Terrile, R. J., Thomas, P., Thompson, W. R., Verbiscer, A., and Veverka, J. 1989. Voyager 2 at Neptune: Imaging science results. *Science* 246:1422–1449.

Smith, E. V., and Gottlieb, D. M. 1974. Solar flux and its variations, *Space Sci. Rev.* 15:771–802.

Soifer, B. T., Neugebauer, G., and Matthews, K. 1980. The 1.5–2.5 micron spectrum of Pluto. *Astrophys. J.* 85:166–167.

Spencer, J. R., Buie, M. W., and Bjoraker, G. L. 1990. Solid methane on Triton and Pluto: 3- to 4-μm spectrophotometry. *Icarus* 88:491–496.

Stansberry, J. A., Lunine, J. I., Hubbard, W. B., Yelle, R. V., and Hunten, D. M. 1994. Mirages and the nature of Pluto's atmosphere. *Icarus* 111:503–513.

Stansberry, J. A., Pisano, D. J., and Yelle, R. V. 1996. The emissivity of volatile ices on Triton and Pluto. *Planet. Space Sci.*, in press.

Stern, S. A., Trafton, L. M., and Gladstone, G. R. 1988. Why is Pluto bright? Implications of the albedo and lightcurve behavior of Pluto. *Icarus* 74:485–498.

Stern, S. A., Brosch, N., Barker, E. S., and Gladstone, G. R. 1991. Rotationally resolved midultraviolet studies of Triton and the Pluto/Charon system I: IUE results. *Icarus* 92:332–341.

Stern, S. A., Weintraub, D. A., and Festou, M. C. 1993. Evidence for a low surface temperature on Pluto from millimeter-wave thermal emission measurements. *Science* 261:1713–1716.

Sykes, M. 1993. Implications of Pluto–Charon radiometry. *Bull. Amer. Astron. Soc.* 25:1138 (abstract).

Sykes, M., Cutri, R., Lebofsky, L., and Binzel, R. 1987. IRAS serendipitous survey observations of Pluto and Charon. *Science* 237:1336–1340.

Tedesco, E. F., Veeder, G. J., Dunbar, R. S., and Lebofsky, L. A. 1987. IRAS constraints on the sizes of Pluto and Charon. *Nature* 327:127–129.

Tholen, D. J., and Buie, M. W. 1988. Circumstances for Pluto–Charon mutual events in 1989. *Astron. J.* 96:1977–1982.

Tholen, D. J., Buie, M. W., Binzel, R. P., and Frueh, M. A. 1987. Improved orbital and physical parameters for the Pluto–Charon system. *Science* 237:512–514.

Trafton, L. 1984. Large seasonal variations in Triton's atmosphere. *Icarus* 58:312–324.

Trafton, L., and Stern, S. A. 1983. On the global distribution of Pluto's atmosphere. *Astrophys. J.* 267:872–881.

Trafton, L., and Stern, S. A. 1994. HST observations of Pluto's UV lightcurve and Charon's UV spectrum. *Bull. Amer. Astron. Soc.* 26:1169 (abstract).

Tryka, K., Brown, R. H., Cruikshank, D. P., Owen, T. C., de Bergh, C., and Geballe, T. R. 1993. Determination of the temperature of nitrogen on Pluto from spectral measurements. *Bull. Amer. Astron. Soc.* 25:1129 (abstract).

Tryka, K., Brown, R. H., Cruikshank, D. P., Owen, T. C., Geballe, T. R., and de Bergh, C. 1994. Temperature of nitrogen ice on Pluto and its implications for

flux measurements. *Icarus* 112:513–527.

Tryka, K., Brown, R. H., and Anicich, V. 1995. Near-infrared absorption coefficients of solid nitrogen as a function of temperature. *Icarus* 116:409–414.

Tyler, G. L., Sweetnam, D. N., Anderson, J. D., Borutzki, S. E., Campbell, J. K., Eshleman, V. R., Gresh, D. L., Gurrola, E. M., Hinson, D. P., Kawashima, N., Kursinski, E. R., Levy, G. S., Lindal, G. F., Lyons, J. R., Marouf, E. A., Rosen, P. A., Simpson, R. A., and Wood, G. E. 1989. Voyager radio science observations at Neptune and Triton. *Science* 246:1466–1473.

Van Thiel, M., Decker, E. D., and Pimentel, G. C. 1957. Infrared studies of hydrogen bonding of water by the matrix isolation technique. *J. Chem. Phys.* 27:486–490.

Verbiscer, A. J., and Veverka, J. 1989. Albedo dichotomy of Rhea: Hapke analysis of Voyager photometry. *Icarus* 82:336–353.

Verbiscer, A. J., and Veverka, J. 1992. Mimas: Photometric roughness and albedo map. *Icarus* 99:63–69.

Warren, S. G. 1984. Optical constants of ice from the ultraviolet to the microwave. *Appl. Opt.* 23:1206–1225.

Watts, A. W., Greeley, R., and Melosh, H. J. 1991. The formation of terrains antipodal to major impacts. *Icarus* 93:159–168.

Weissman, P. R., and Stern, S. A. 1994. The impactor flux in the Pluto–Charon system. *Icarus* 111:378–386.

Weissman, P. R., Dobrovolskis, A. R., and Stern, S. A. 1989. Constraints on impact rates in the Pluto–Charon system and the population of the Kuiper comet belt. *Geophys. Res. Lett.* 16:1241–1244.

Yelle, R. V., and Lunine, J. I. 1989. Evidence for a molecule heavier than methane in the atmosphere of Pluto. *Nature* 339:288–290.

Yelle, R. V., Lunine, J. I., and Hunten, D. M. 1991. Energy balance and plume dynamics in Triton's lower atmosphere. *Icarus* 89:347–356.

Young, E., and Binzel R. P. 1993. Comparative mapping of Pluto's sub-Charon hemisphere: Three least squares models based on mutual event lightcurves. *Icarus* 102:134–149.

Young, L., Elliot, J., Tokunaga, A., de Bergh, C., and Owen, T. C. 1996. Detection of gaseous methane on Pluto. *Icarus*, submitted.